UC Santa Barbara

UC Santa Barbara Previously Published Works

Title

The Intersection of Interfacial Forces and Electrochemical Reactions

Permalink

https://escholarship.org/uc/item/7zh210qn

Journal

The Journal of Physical Chemistry B, 117(51)

ISSN

1520-6106

Authors

Israelachvili, Jacob N
Kristiansen, Kai
Gebbie, Matthew A
et al.

Publication Date

2013-12-27

DOI

10.1021/jp408144g

Copyright Information

This work is made available under the terms of a Creative Commons Attribution-NonCommercial License, availalbe at https://creativecommons.org/licenses/by-nc/4.0/

Peer reviewed

eScholarship.org Powered by the California Digital Library
University of California

JPCBFK

DECEMBER 26, 2013
VOLUME 117
NUMBER 51

pubs.acs.org/JPCB

THE JOURNAL OF PHYSICAL CHEMISTRY B

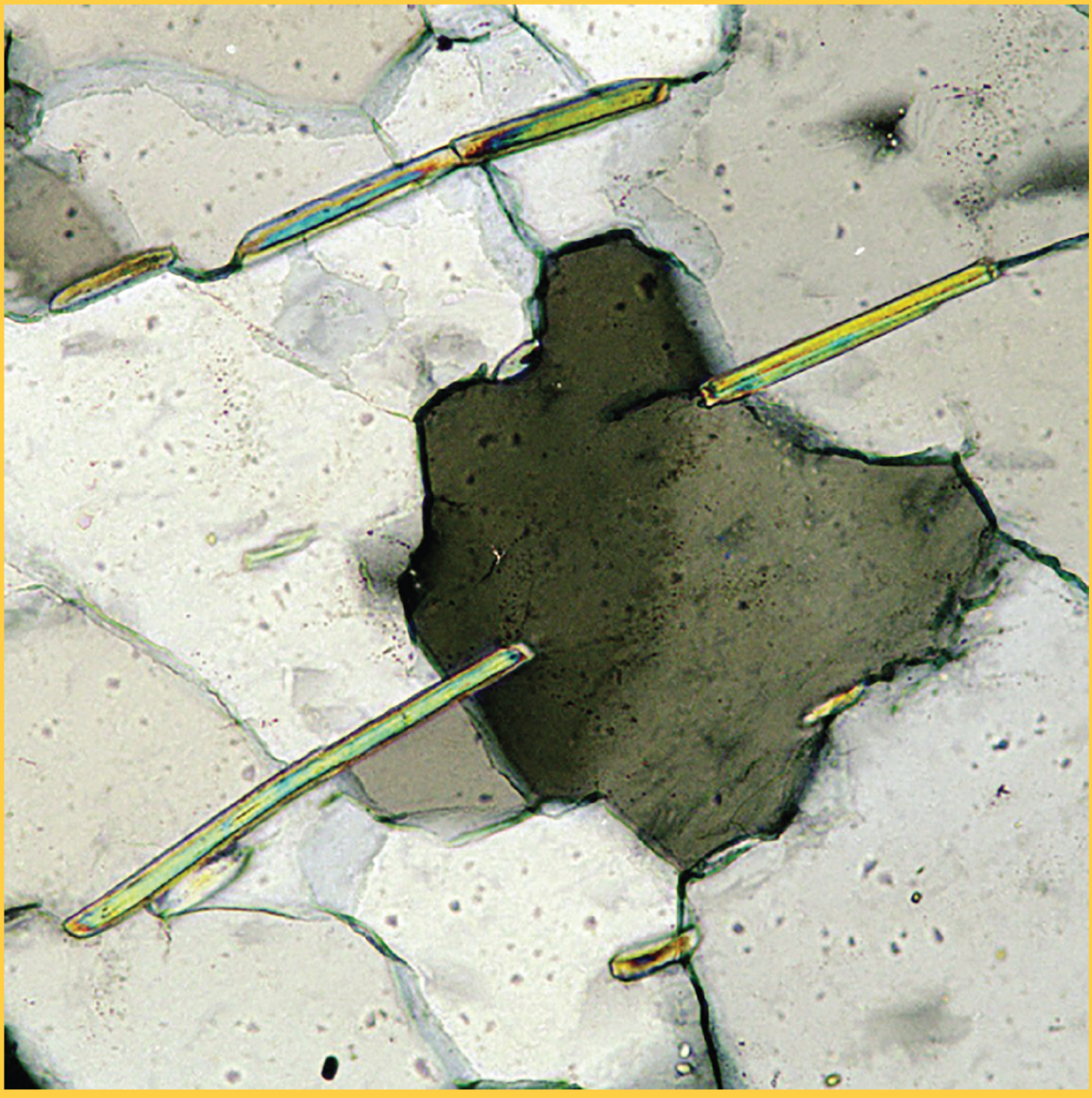

Photomicrograph (crossed nicols) of Detrital Muscovite Mica That Links Quartz Grains in Flexible Sandstone (see page 5A)

BIOPHYSICAL CHEMISTRY, BIOMATERIALS, LIQUIDS, AND SOFT MATTER

ACS Publications
MOST TRUSTED. MOST CITED. MOST READ.

www.acs.org

THE JOURNAL OF PHYSICAL CHEMISTRY B

Feature Article

pubs.acs.org/JPCB

The Intersection of Interfacial Forces and Electrochemical Reactions

Jacob N. Israelachvili,*[,†,‡] Kai Kristiansen,[†] Matthew A. Gebbie,[‡] Dong Woog Lee,[†] Stephen H. Donaldson, Jr.,[†] Saurabh Das,[†] Michael V. Rapp,[†] Xavier Banquy,[§] Markus Valtiner,[∥] and Jing Yu[⊥]

[†]Department of Chemical Engineering, University of California at Santa Barbara, Santa Barbara, California 93106, United States

[‡]Materials Department, University of California at Santa Barbara, Santa Barbara, California 93106, United States

[§]Faculty of Pharmacy, Universite de Montreal, Succursale Centre Ville Montreal, Quebec H3C 3J7, Canada

[∥]Interface Chemistry and Surface Engineering, Max-Planck-Institut für Eisenforschung GmbH, 40237 Düsseldorf, Germany

[⊥]NanoSystems Biology Cancer Center and Kavli Nanoscience Institute, Division of Chemistry and Chemical Engineering, California Institute of Technology, Pasadena, California 91125, United States

Supporting Information

ABSTRACT: We review recent developments in experimental techniques that simultaneously combine measurements of the interaction forces or energies between two extended surfaces immersed in electrolyte solutions—primarily aqueous—with simultaneous monitoring of their (electro)chemical reactions and controlling the electrochemical surface potential of at least one of the surfaces. Combination of these complementary techniques allows for simultaneous real time monitoring of angstrom level changes in surface thickness and roughness, surface−surface interaction energies, and charge and mass transferred via electrochemical reactions, dissolution, and adsorption, and/or charging of electric double layers. These techniques employ the surface forces apparatus (SFA) combined with various "electrochemical attachments" for *in situ* measurements of various physical and (electro)chemical properties (e.g., cyclic voltammetry), optical imaging, and electric potentials and currents generated naturally during an interaction, as well as when electric fields (potential differences) are applied between the surfaces and/or solution—in some cases allowing for the chemical reaction equation to be unambiguously determined. We discuss how the physical interactions between two different surfaces when brought close to each other (<10 nm) can affect their chemistry, and suggest further extensions of these techniques to biological systems and simultaneous *in situ* spectroscopic measurements for chemical analysis.

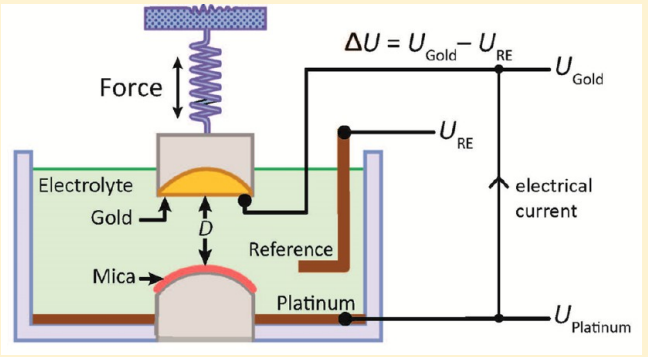

1. INTRODUCTION

Chemical reactions can occur either inside the bulk phase of a substance, which could be in the vapor, liquid, or solid phase, or at a surface or interface between two bulk phases. By convention, the term *surface* refers to a condensed phase exposed to vapor, for example, a solid or liquid surface in air, while the term *interface* refers to the boundary between two condensed phases, for example, a solid−liquid or liquid−liquid interface. However, many authors use the term surface to cover both surfaces and interfaces, for example, "...the surfaces of the colloidal particles..." or "...the distance between the two membrane surfaces..." even when these (interfaces) are in solution, and we shall be doing the same here when there is no likelihood of ambiguity.

In this article, we focus mainly on the chemical and electrochemical reactions involving interfaces, either single (isolated) interfaces or two interfaces close together in electrolyte solution, where the proximity of another interface has an effect on these reactions. The way one interface can affect the *chemical processes* of another, nearby interface is usually through non-covalent *physical* interaction forces (also colloidal forces), such as the long-range van der Waals and—if the surfaces are charged in water—electrostatic (double layer) forces. These two latter forces are known as the DLVO forces after Derjaguin−Landau−Verwey−Overbeek[1] and form the basis of understanding the long-range (>2 nm) interactions of colloidal particles and biological surfaces, e.g., of vesicles or cell membranes. The interaction energies associated with colloidal forces are usually much weaker than the energies associated with chemical reactions, but as has recently be found, they can have a surprisingly large effect on reaction rates.

Closer in, at surface separations below 1−2 nm but still not at contact separations (say, <0.3 nm), various "solvation" (solvent structural) forces, for example, due to water layering in

Received: August 14, 2013
Revised: November 13, 2013
Published: November 15, 2013

 © 2013 American Chemical Society dx.doi.org/10.1021/jp408144g | J. Phys. Chem. B 2013, 117, 16369−16387

aqueous solutions, hydration (H-bonding) effects, or ionic binding, have much larger interaction energies which give rise to additional forces. These forces can be attractive, repulsive, or oscillatory[2] and often exhibit some covalent bond characteristics such as directionality and stoichiometry. The effects of these shorter-range interactions can be more dramatic, affecting both the reaction pathways as well as their rates.

Many systems involving particles in solution such as colloidal suspensions, food emulsions, clay slurries, gels, personal care consumer products, and biological structures such as intracellular organelles are highly concentrated such that no surface is farther away from another surface than about 10 nm. In other words, every surface is interacting with, i.e., "feels" the presence of, another surface via long-range colloidal or short-range solvation forces. The question arises: What effect do these interaction forces (or energies) have on the chemical reactions occurring at the interfaces?

Of course, electrochemical reactions can occur at both single (isolated) as well as two *well-separated*, but still coupled, surfaces, for example, the action of a battery (also electrolytic or galvanic cells) where a potential difference (voltage) is created between two different (electrode) surfaces that are immersed in the same electrolyte solution. When the two electrode surfaces are externally connected via a wire or circuit, the potential difference drives a flow of electrons through the wire accompanied by the conduction (transfer) of ions from one of the surfaces to the other through the intervening electrolyte, for example, metal cations like Na^+ migrating to the cathode to be reduced and halogen anions like Cl^- migrating to the anode to be oxidized, resulting in the buildup of neutral species at each surface. Other examples include the corrosion of metal surfaces, which is believed to be similar to the action of electrolytic cells, and electro-polishing and electro-deposition (electro-plating), where now the application of an external potential between two surfaces causes the dissolution or deposition of material on one or both surfaces.

All of the above phenomena are well-understood effects that do not depend on the close proximity or interaction forces between the surfaces. Our focus here will be on cases where the close approach of two surfaces is seen to impact chemical reactions at surfaces—whether the chemistry is modified from the "well-separated" situation described above or generated by the interaction—and how these effects are related.

The idea that some interactions are responsible for modifying or generating chemical reactions at one or both of two closely apposed surfaces is not new. However, deciding which interaction is responsible—whether mechanical forces of abrasion (friction), electrical forces due to high local fields or ionic bridges, steric or solvation forces due to solvent-mediated adhesion—has usually not been resolved. Or the phenomenon may have been attributed to the wrong interaction, and we illustrate two important examples of this here—the phenomena of chemical mechanical polishing (CMP) and pressure solution (which are discussed in more detail later).

Figure 1 shows highly mirror polished surfaces of blades made of hard steel that were initially rough after use in excavating soft clay slurries of amorphous silica in moist soil. Similar mirror finishes (down to <5 nm) are attained when hard silicon, sapphire, and even diamond surfaces are rubbed with much softer materials while immersed in electrolyte solution. The mechanism is referred to as "chemical mechanical polishing" (CMP); however, there is never any indication of mechanical abrasion, for example, scratch marks or friction tracks that are the usual signature of mechanical abrasion. As discussed in section 4, such processes are more likely to be due to "non-contact" electrochemical dissolution reactions than actual friction abrasion, involving both the colloidal interaction forces between the two surfaces in the (aqueous) solution and the electrochemical reaction between the two (electrochemically different) surfaces.

Figure 1. An example of "chemical mechanical polishing" (CMP) here showing hard steel being highly polished, with no scratch marks, by a wet slurry of soft amorphous silica. (Photo taken at the Diatomite Quarry, Lompoc, California. Unpublished photo, J. R. Boles, UCSB, Earth Science.)

Our second example involves the natural geological phenomenon of "pressure solution"—the mechanism that is traditionally used to explain the morphogenesis or shape evolution of rocks. The idea is that, over millions of years, a rock surface dissolves and/or deforms slowly but plastically due to the (lithostatic) pressure from other nearby rocks. This model again invokes purely mechanical stresses and not some chemical reaction. Many rock formations (e.g., strata) are clearly due to slowly deforming layers subjected to such mechanical stresses. However, as shown in Figure 2, when subjected to high resolution microscopic imaging, there are

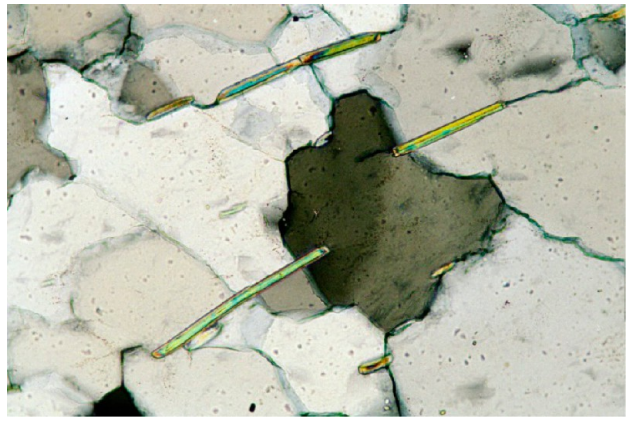

Figure 2. Photomicrograph (crossed nicols polarizers microscope) of soft mica flakes (in green) about 0.5 mm long that have penetrated into hard quartz grains—an example of "pressure solution" in geological rock morphologies, measured at the molecular level using the EC-SFA. (Sample from Appalachian mountain area, USA. Unpublished photomicrograph from J. R. Boles, UCSB Earth Science collection.)

dx.doi.org/10.1021/jp408144g | J. Phys. Chem. B 2013, 117, 16369−16387

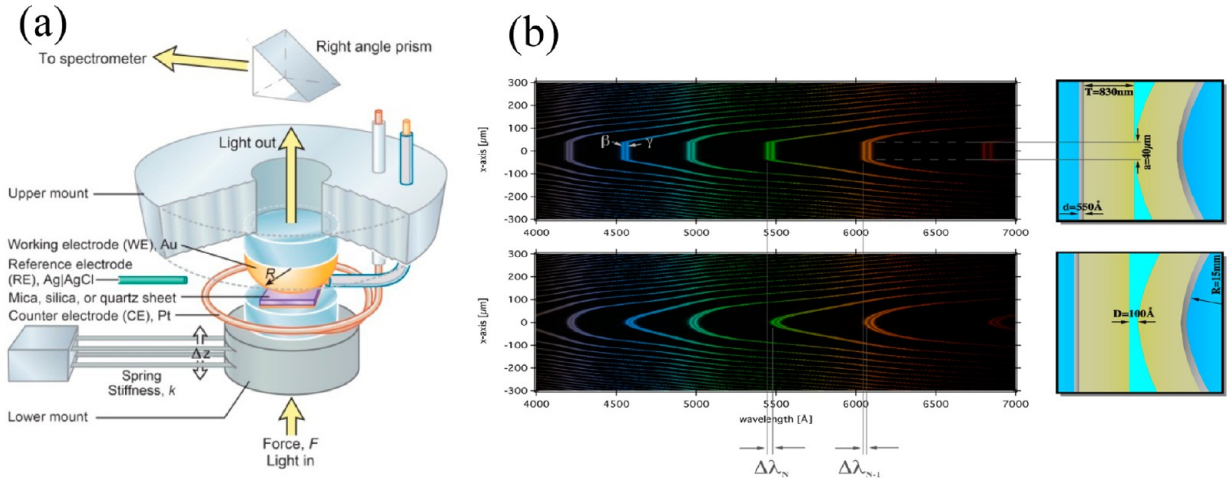

Figure 3. (a) The electrochemical surface forces apparatus (EC-SFA) has the capabilities of *in situ* measurement of forces and simultaneous measurement and control of potential differences, currents, and surface (electro)chemistries. (b) FECO interference fringe patterns (left panels) from the crossed-cylinder or sphere-on-flat geometry (right panels) as seen in the exit port of a normal spectrometer. The vertical and horizontal axes of the spectrograms correspond to the lateral distance (on the surfaces) and the normal distance (surface separation) at each location, respectively, and thus give the profile of the two surfaces. The adhesion forces between the surfaces coupled to the finite elastic compliance of the (originally curved) surfaces and their substrates produces the flattening of the FECO fringes at contact, where the wavelength defines $D = 0$ (top panels). When the surfaces are separated from adhesive contact, the fringes move to longer wavelengths (to the right) and regain their rounded (curved) shapes. The absolute distance of separation, D, at any location of the surfaces can be calculated on the basis of the shift in the wavelength from that of the contact fringe. More on the SFA and the FECO optical technique can be found in refs 7 and 8.

clear indications of soft materials, like mica flakes, that flatten hard materials or penetrate into them, like crystalline quartz, with no apparent deformation of the *soft material*. In such cases, again, the observed flattening and penetration of the hard material (silica) appears to be due to chemical dissolution brought about by the close proximity of the mica flakes, rather than mechanical pressure or frictional abrasion.

The nature of the (electro)chemical reactions responsible for the above two phenomena is subtle, and is examined in some detail in this article, together with six other phenomena where close proximity of two surfaces, the interaction forces (both the normal and shear or frictional forces), and the (electro)-chemical reactions occurring at the two interfaces are correlated. We consider situations where electric potentials and currents are generated naturally during an interaction, as well as when electric fields are applied, and we also consider non-aqueous liquids. We find situations where surfaces are dissolved away, and where material is adsorbed on them; situations where surfaces become smoother, and where they become flattened. We will also see situations where the electrochemical reaction can be followed in situ "quantitatively", which allows for the determination of the corresponding electrochemical reaction equation.

We end with a discussion of possible future extensions of these techniques, in particular (i) to simultaneous *in situ* spectroscopic measurements for chemical analysis such as IR, FTIR, SHG, and SFG, and (ii) biological systems, for example, two cell surfaces or membranes, where such effects are likely to be particularly important because such surfaces are often closer than 5−10 nm.

2. ELECTROCHEMICAL ATTACHMENTS FOR THE SURFACE FORCES APPARATUS (EC-SFA)

The design of an apparatus enabling the measurements of surface−surface interaction forces with simultaneous *in situ* external control of the surface potentials and/or surface charge densities was a key development for the process of gaining deeper insights into the complex relationships between physical colloid interactions and surface electrochemistry properties, as well as the specific ions adsorbed on, and the electrochemical reactions at, the surfaces. This new range for such electrochemical studies became feasible when the Vanderlick group[3] and others[4,5] combined electrochemical control/measuring techniques with simultaneous measurements of the interaction forces and absolute distance measurement capabilities of the SFA. Figure 3a shows the realization of a recently developed electrochemical cell (or attachment) for the surface forces apparatus (the EC-SFA).

The EC-SFA setup shown in Figure 3a has three main electrodes, where the upper Au surface (evaporated or mica-templated film of thickness 42.5 nm) acts as the working electrode (WE). The use of the mica-templated Au provides an atomically smooth surface that is essential for precise interfacial energy measurements.[5] The counter electrode (CE) is in close proximity to and surrounds the working electrode, and can either be a Pt ring (as shown in Figure 3a), an evaporated Pt layer on a surrounding disk (see Figure 8a later), or a disk of Pt mesh. The reference electrode (RE) is typically a Ag|AgCl electrode, where the measuring point is close to the working electrode; however, other reference electrodes can easily be substituted for Ag|AgCl. The electrochemical cell shown in Figure 3a is well-behaved, as demonstrated by cyclic voltammogram (CV) measurements (see Figure 10a later) that replicated the CV obtained in other published electrochemical cells.[6] The electrochemical cell can also readily be used for any other analytical electrochemistry techniques, for example, impedance spectroscopy.

The upper Au surface is also optically reflective and is an integral part of the multiple beam interferometric (MBI) method used for measuring the distance between the two surfaces to angstrom resolution in the SFA. The lower surface (usually a sheet of molecularly smooth mica, but can also be silica, quartz, sapphire, or other transparent material) has a

dx.doi.org/10.1021/jp408144g | J. Phys. Chem. B 2013, 117, 16369−16387

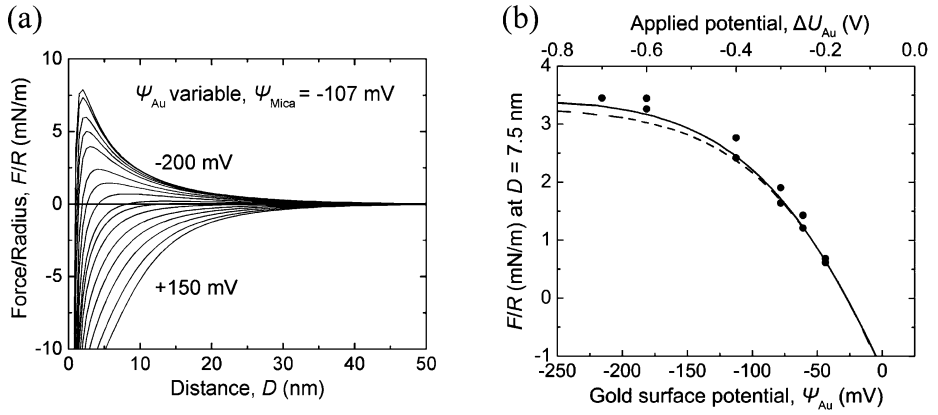

Figure 4. (a) DLVO predictions of surface forces (normalized by radius of curvature) between mica and gold surfaces immersed in 10^{-3} M aqueous electrolyte solution: the corresponding Debye length is 9.6 nm. The mica is set as a constant charge with a surface potential of $\psi_{mica} = -107$ mV, as determined through control experiments. Interactions were calculated for gold surface potentials of (from top to bottom) −200, −185, −155, −135, −115, −85, −65, −45, −25, −15, 0, 20, 40, 65, 100, and 150 mV. (b) Magnitude of double layer forces at a distance of $D = 7.5$ nm, where van der Waals forces are negligible. Points correspond to experimental data, and lines correspond to the same calculations as in panel a. Measured double layer forces (DLVO forces) were in agreement with the theoretical predictions for mica−gold separation distances of greater than 7.5 nm, and forces were found to saturate for applied potentials more negative than ΔU_{Au} −0.6 V versus a gold quasi-reference electrode (QRE). Separate control experiments showed that the gold QREs exhibit open circuit potentials of −0.310 V versus Ag/AgCl (adapted from ref 3).

reflective film on the back (55 nm silver or 42.5 nm gold provide suitable reflection coefficients for MBI) and is mounted on a double cantilever (force-measuring) spring with a known spring constant, k. The incident white light passes through the lower surface (see Figure 3a), and constructively and destructively interferes by reflecting off of the thin metallic layers on the lower and upper surfaces. The interfering light beam is guided to a spectrometer that diffracts the light into separate wavelengths or "multiple beam interference fringes", known as fringes of equal chromatic order (FECO). Two examples of the FECO fringe patterns for two surfaces, in adhesive contact and separated, are shown in Figure 3b. The two surfaces are mounted in a crossed-cylinder or sphere-on-flat configuration, which are locally geometrically equivalent. The calculations of the surface separation and surface shape profiles (including the contact area) from the FECO profiles are described elsewhere.[7−9] The EC-SFA inherits the stability of the SFA allowing for long-term and equilibrium measurements.

Electrostatic double layer forces depend on the surface potentials or charge densities of the two surfaces, which can be different (asymmetric surfaces). With the EC-SFA attachment, the electrochemical potential (not to be confused with the electric double layer potential, called the outer Helmhotz plane (OHP) potential) of one of the surfaces (the working electrode surface) can be accurately controlled, and the current through that surface can be precisely measured. The apposing surface—usually an atomically smooth mica surface—will generally have a different, and also measurable, surface potential.

The double layer force F between two electrically asymmetric surfaces at a separation distance D and at constant low surface potentials (<25 mV) is given by the well-known Hogg−Healy−Fuerstenau (HHF) equation:[10]

$$\frac{F(D)}{R} \approx \frac{4\pi\varepsilon\varepsilon_0\kappa[(e^{\kappa D} + e^{-\kappa D})\psi_1\psi_2 - (\psi_1^2 + \psi_2^2)]}{(e^{\kappa D} - e^{-\kappa D})^2} \quad (1)$$

where R is the radius of the upper sphere, ψ_1 and ψ_2 are the OHP surface potentials, $1/\kappa$ is the Debye length, ε_0 is the permittivity of free space, and ε is the relative permittivity of the medium between the surfaces. Importantly, the actual surface OHP potential of the working electrode that is used to analyze the magnitude of measured double layer forces is not exactly the same as the applied potential (from the external source, like a potentiostat); the OHP potential instead depends on the applied electrochemical potential in a complex manner that depends on the surface chemistry, ion chemistry, and reference electrode selection.[11] The equations for the double layer forces at constant surface charge densities, mixed boundary conditions, and charge regulation can be found elsewhere.[12]

Finally, in the EC-SFA, the lower (inert or passive/inactive mica or silica) surface can be replaced by a conductive surface whose potential can also be controlled, thereby producing two conductive (as well as optically reflective) surfaces facing each other. This configuration allows for controlled electric fields to be applied across the two surfaces (or interfaces) in both aqueous and non-aqueous liquids.

3. ELECTRIC DOUBLE LAYER FORCES CONTROLLED BY EXTERNALLY APPLIED POTENTIALS

The EC-SFA was first used in 2001 to explore the relationship between externally applied electrochemical potentials and electric double layer interaction forces between two surfaces—mica and polycrystalline gold electrodes—in dilute aqueous electrolyte solutions (Figure 4).[3] In particular, Fréchette and Vanderlick tested whether the DLVO theory of colloidal forces could be utilized to describe interaction forces as the electrochemical potentials of the gold surfaces were controlled externally. All of the potentials studied were in a range where the gold behaved as an ideally polarizable electrode, and mica acquires a negative surface charge from the dissociation of K^+ ions when immersed in aqueous solutions of pH 5.5.[3] Figure 4a shows DLVO theoretical calculations that illustrate how the interaction forces are expected to vary as the outer Helmholtz plane (OHP) potential of the gold surface is changed from highly negative (repulsive interactions) to highly positive (attractive interactions) values.[3] The relationship between the applied potentials and the surface OHP potentials can be found in Figure 4b.

dx.doi.org/10.1021/jp408144g | J. Phys. Chem. B 2013, 117, 16369−16387

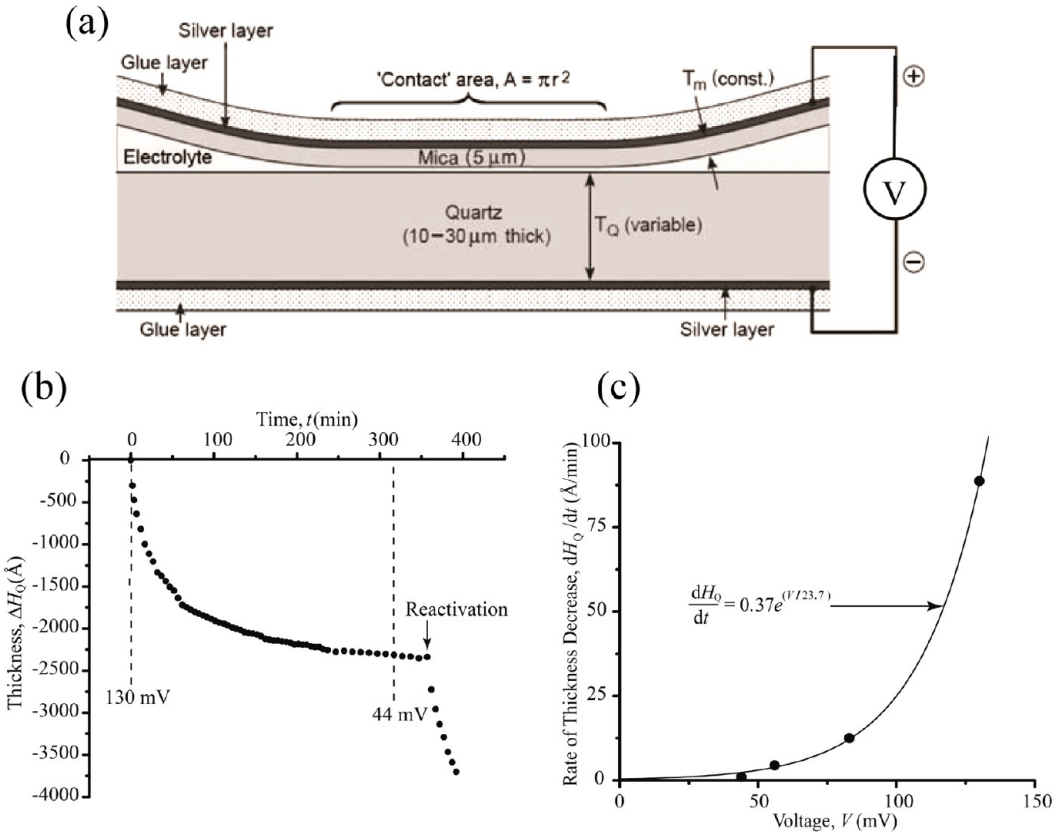

Figure 5. (a) Schematic of the experimental geometry of the surfaces and potential-measuring electrode surfaces in the SFA used for measuring the dissolution of one of the surfaces (the lower quartz surface in this case) induced by the close proximity (overlap of electric double layers) of another surface (the upper mica surface in this case) having a more negative surface potential, V. This electrochemical potential difference can be natural to the two surfaces (depending on the solution conditions) or externally applied, as illustrated in Figure 6a. In the above geometry, the 55 nm thick silver layers serve both as electrically conducting electrodes and as optically reflecting layers for imaging the surfaces (using multiple beam interference fringes, Newton's rings, or simple optical microscopy). (b) Typical evolution of the pressure solution type of experiments (muscovite mica pressed against a quartz surface) using an SFA. The dissolution of the quartz is seen as a decrease of its thickness, ΔH_Q, as a function of the time, t. The voltage drop across the quartz and mica, V, is also recorded, and shows (c) a higher rate of thickness decrease, dH_Q/dt, at higher recordings of the voltage drop. The correlation between dH_Q/dt and V is well described by an exponential function similar to the Nernst equation. Reprinted with permission from ref 20. Copyright 2009 Elsevier.

DLVO theory was found to do an excellent job of predicting interaction forces when the mica−gold separation distances were greater than about one Debye length,[3] and several subsequent studies of interfacial forces under external potential control reached similar conclusions.[5,11,13,14] Further, the magnitudes of the double layer forces were found to saturate at electrochemical potentials that are large in magnitude: increasing the (negative) magnitude of the applied potential from −600 to −700 mV resulted in no measurable change in the magnitude of the measured double layer repulsion (Figure 4b).[3] The presence of a force saturation regime—where large increases in surface potentials lead to marginal increases in double layer forces—is also predicted by DLVO theory (Figure 4a).[3]

When the applied potentials were small in (negative) magnitude relative to the natural potential (open circuit potential) of the gold surfaces—gold OHP potentials between −85 and −25 mV—the measured forces were small in magnitude and exhibited only slight repulsive deviations from DLVO theory before jumping into adhesive contact.[3] Since the magnitude of adhesive forces predicted from DLVO theory is highly sensitive to both the effective Hamaker constant as well as the absolute, angstrom-scale distance at which the interaction is "cutoff" (i.e., the separation of mica and gold atoms in contact), Fréchette and Vanderlick concluded that DLVO theory could likely be utilized to model the adhesive forces but noted that any predictions would be highly sensitive to parameter selections.[3] Fréchette and Vanderlick later used results from additional EC-SFA experiments to develop a more robust electrocapillary model for predicting the magnitude of adhesive (or repulsive) interactions between mica and gold surfaces under external potential control.[13]

As the electrochemical potentials applied to the gold surface were increased to large (negative) magnitudes—corresponding to gold OHP potentials more negative than −100 mV—the short-range interaction forces were found to be substantially more repulsive than expected from DLVO theory, with the mica−gold system exhibiting purely repulsive interaction forces, even down to final "hard contact".[3] These deviations were attributed primarily to surface roughness effects[3]—in agreement with subsequent electrochemical AFM and SFA measurements[5,11,13−15]—however, later work also demonstrated the importance of specific ion−surface adsorption effects in causing short-range deviations from the predictions of DLVO theory.[5,11,14,15]

For example, recent work by Valtiner et al.[5] shows that both the saturation of long-range double layer forces and the magnitudes and ranges of short-range deviations from DLVO

dx.doi.org/10.1021/jp408144g | J. Phys. Chem. B 2013, 117, 16369−16387

theory are intimately tied to the roughness of electrode surfaces. At the atomic level, rough surfaces expose significantly more surface area (per macroscopic unit area) to electrolyte solutions than atomically smooth surfaces. Thus, counterions have a larger surface area available for specific binding and can more effectively neutralize electrochemical potentials applied to rough surfaces, as compared to atomically smooth surfaces.[5] Several other studies also indicate that ion−surface binding/condensation effects, i.e., the increased buildup of surface bound ions, play significant roles in modifying interaction and especially short-range and adhesion forces between two surfaces.[5,11,14,15] Indeed, in 2001, Wang and Bard had already used AFM with *in situ* electrochemical control of polycrystalline gold substrates to reach the conclusion that ion binding and condensation effects were a major cause of deviations in force measurements from the Gouy−Chapman−Stern model of electric double layers utilized in DLVO theory.[15]

In general, these short-range deviations from DLVO theory can be accounted for by using empirical models incorporating exponentially decaying steric repulsion terms superimposed with DLVO theory,[5,11] for example, one distinct term accounting for the compression of asperities (rough surfaces) and another accounting for the compression of surface-bound ions and/or solvent molecules. These empirical models are analogous to the "hydration repulsion" models developed to account for cation binding at mica surfaces,[16] and the parameters for these models cannot currently be predicted *a priori*.

4. NATURAL ELECTROCHEMICAL REACTIONS—PRESSURE SOLUTION

Many weathering phenomena of natural and man-made materials are due to electrochemical reactions, which depend on apposing surfaces of different materials in close proximity, in different electrolyte solution. The proximity of two surfaces leads to either an electrostatic potential drop or an overlapping double layer interaction between the two surfaces that can enhance the reaction rate (i.e., lower the activation energy for the reaction) of one of the surfaces. In addition, electrolytes in the solution can form complexes with the material or can be a catalyst for the reactions. Typical examples of electrochemical weathering phenomena are the pressure solution in geological formations (see Figure 2), crevice corrosion, chemical mechanical polishing,[17] the claws of the excavator (see Figure 1), stability of containers of nuclear waste disposal,[18] and wall stability in micro- and nanofluidic devices.[19] In this section, we will discuss laboratory experiments imitating the pressure solution phenomenon that occurs naturally in geological formations, while, in the following section (section 5), we will employ the EC-SFA to gain more insight into the importance of the electrochemical surface potential on dissolution to provide crucial information about the pressure solution phenomenon and possibly to the other above-mentioned phenomena as well.

The enhanced dissolution rate of quartz in contact with micaceous (muscovite, illite, smectite) materials is a characteristic element of the pressure solution phenomenon.[20,21] The cause of this dissolution has long baffled the geological community, and in spite of their apparent importance, several geological processes are not yet well-understood, e.g., pitting and indentation at grain contacts, formation of stylolites, overgrowths, cleavage, and the deformation of metamorphic rocks.[20] Geological observations, like the sample shown in Figure 2, initiated the use of the SFA to study the pressure solution phenomenon.[22] Figure 5a shows a typical realization of these types of experiments where the thickness change of a thin slide of quartz is measured over time when a muscovite mica flake is pressed against it (at 2−3 atm pressure) while immersed in a 30 mM $CaCl_2$ solution of pH 3. The dissolution rate can be measured as low as 0.01 nm/min. In addition to the thickness change, the voltage drop between the back-silvered films of the mica and the quartz is measured simultaneously. Figure 5b shows the measured changes in the quartz thickness with time, ΔH_Q vs t undergoing natural pressure solution (no external applied electric field or potentials). Also shown in Figure 5b are selected measured electrostatic potentials V during the measurement.

Figure 5c shows that the quartz (Z-cut quartz crystal) dissolution rate (dH_Q/dt) when in close proximity to muscovite mica grows roughly exponentially with the electrostatic potential difference V:

$$\frac{dH_Q}{dt} = Ae^{V/V_0} \tag{2}$$

where in these experiments A = 0.37 Å/min ≈ 20 μm/yr and V_0 = 23.7 mV. This is very close to the Nernst equation:

$$\text{Dissolution rate} \propto e^{eV/kT} \tag{3}$$

where kT/e = 25.8 mV at room temperature, with e being the electric charge, T the absolute temperature, and k Boltzmann's constant.

The pressure solution phenomenon is a complex system where several variables can change the dissolution rate of the quartz. The dissolution rate shows some dependence on the crystallographic orientation of the quartz crystal.[23] Displacement agitation normal to the surfaces shows no effect, while shearing mica against quartz increases the dissolution rate considerably.[20] The effect of ions in the aqueous solution will be discussed in the next section.

One of the most intriguing effects on the dissolution rate of quartz is due to the difference in the electric surface potential of the two surfaces in proximity, as seen from Figure 5c. Control experiments with equal electric surface potential, like mica−mica and quartz−quartz, show no change in thickness. The geological samples, like Figure 2, show enhanced dissolution of quartz in the proximity of more negatively charged surfaces, like muscovite mica, in electrolyte solutions with ionic strength and pH in the geological range (few ones to tens of mM, and pH 4.5−9, respectively). Geological observations of other materials with more positive surface potentials than quartz, like zircon and magnetite, show an inhibition of quartz dissolution.[6] This dependency of the electrochemical surface potential of the apposing surface on the dissolution rate is the background for developing the electrochemical cell for the surface forces apparatus and the basis for the experiments and discussion in the next section.

5. "PRESSURE (DIS)SOLUTION" UNDER EXTERNAL ELECTRIC POTENTIAL CONTROL

The geological samples (Figure 2) and experimental results (Figure 5) of muscovite mica pressed against a quartz surface show an enhanced dissolution rate of quartz. This enhanced dissolution of quartz occurs in experiments even at low pressure (2−3 atm) and temperature (23 °C) compared to the high pressure and temperature experienced by rock formations over

dx.doi.org/10.1021/jp408144g | J. Phys. Chem. B 2013, 117, 16369−16387

millions of years. These experiments, together with the geological observations that more positively charged surfaces like zircon and magnetite inhibit quartz dissolution, suggest that other physiochemical explanations than the previously thought explanations[24] of pressure or strain are responsible for the enhanced dissolution of quartz. The overlapping electrical double layer (i.e., asymmetric surface potentials) was proposed to be one of the main mechanisms.[20,25] The hypothesis that the dissolution rate of a quartz surface is changed by an apposing electrically charged surface in close proximity lead us to the development of the electrochemical cell attachment for the SFA (EC-SFA). Figures 3 and 6a show schematics of the setup

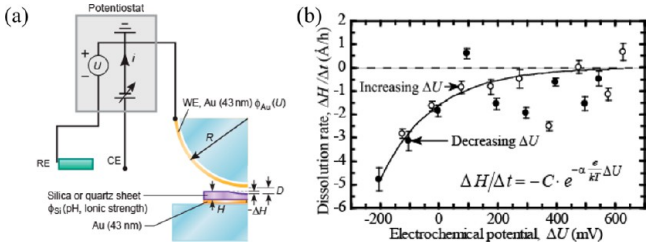

Figure 6. (a) The three-electrode setup with the upper gold surface as the working electrode allows control of the potential of the surface apposing a silica or quartz surface, while the SFA technique allows one to simultaneously monitor the thickness of the silica or quartz surface in real time. (b) Measurements of the dissolution rates of silica surfaces over a 2 h period at each potential show an enhanced dissolution of the silica at more negative potentials of the gold electrode, and that the dissolution rate is well described by the Butler–Volmer Arrhenius-like equation. A detailed analysis of the reaction mechanics given in ref 22 provides a good prediction of the constant C = 0.16 nm/h. The fitting parameter is α = 0.14. Reprinted with permission from ref 6. Copyright 2011 Elsevier.

where the lower surface is the quartz or amorphous silica that we monitor in real time using our FECO technique and the upper gold surface is the working electrode, where we may vary the surface potential, and hence the electric double layer.

The generally accepted chemical reaction of silica dissolution in an aqueous electrolyte is[26,27]

$$SiO_2(s) + 2H_2O(l) \rightarrow Si(OH)_4(aq) \quad (4)$$

It should be noted that the exact reaction equation is yet to be fully characterized. Assuming—based on the chemical reaction of eq 4—an Arrhenius type of dissolution rate that is exponential proportional to activation energy E_a, the temporal change in the thickness of the silica is given by[6]

$$\frac{\Delta H}{\Delta t} = -Ce^{-\alpha(e/k_BT)\Delta U} \quad (5)$$

where k_B is the Boltzmann factor, T is the temperature, e is the elementary charge, α is a transfer factor, and ΔU is the potential of the gold surface referenced to the potential of zero charge of the silica surface U_{PZC}. U_{PZC} is found by fitting eq 1 to the force–distance profiles for several potentials of the gold surface. The activation energy for bond hydrolysis is modified to first order by adding a term proportional to the applied potential:

$$E_a = E_{a,0}(P, D) + \alpha e\Delta U(P, c_i, I, \text{pH}) \quad (6)$$

The value of $\alpha\Delta U$ is approximately the actual surface potential,[5] and itself depends on the contact pressure P, concentration of ions c_i of species i, ionic strength I, and pH of the solution. The zeroth term (no external voltage) of the activation energy $E_{a,0}$ is dependent on the pressure P and the separation distance D. The prefactor C is found to be[6]

$$C = C_0e^{-(1/k_BT)E_{a,0}} \quad (7)$$

where C_0 is a constant that depends on material properties of the silica and the contact area of the silica–gold system. Equation 5 is similar to the Butler–Volmer equation[28]—one of the fundamental relationships in electrochemical kinetics—that describes how the ion or mass current on an electrode depends on the electrode potential.

Figure 6b shows the dissolution rate of amorphous silica ($\Delta H/\Delta t$) as a function of the potential of the apposing gold surface ΔU. The surfaces were immersed in a 30 mM $Ca(NO_3)_2$ aqueous solution at pH 3 and at room temperature. For each data point (i.e., at each potential), the change of the thickness of the silica ΔH was measured over a time period of 2 h. The data in Figure 6b fit well to the Butler–Volmer Arrhenius-like equation (eq 5).[6]

The role of cations in the electrolyte solution are important for the dissolution process; however, the exact mechanism is not currently known. We have observed that divalent cations (e.g., calcium) increase the dissolution rate compared to monovalent cations (e.g., sodium),[20] while experiments by Dove[29] observed rate dependence on the type and concentration of the cations. The dependency of cation type and concentration leads us to believe that these cations have a catalytic effect on the dissolution process, as the positive ions can form bonds with negatively charged dangling bonds at the silica surface or even break up Si–O bonds at the surface. The probability of cations forming bonds with the silica surface can be high considering the fact that the concentration of cations (e.g., calcium) can be very high near the silica surface—it can be several molar even though the bulk concentration is in tens of millimolar—due to the exponential distribution close to a negatively charged surface (e.g., silica).[2]

A low value of the pH in the solution is believed to have an initiator role on the dissolution rate. The excess of protons (hydronium) can have a catalytic effect, just like cations, and protons can also access the surface easier than cations due to its small size. Experiments show similar dissolution rates for silica immersed in pH 3 and in pH 7 as long as the silica surfaces were prepared in pH 3 solutions for an hour before an experiment (and replaced with pH 7 solution immediately before the experiment).[20]

These results demonstrate that, for the dissolution of quartz in geological samples, electrochemical effects are more pronounced than the effects of pressure. High pressure on quartz and silica glass induces mechanical strain and overlapping electric double layers, as well as smaller separation distance D. Both mechanical strain and overlapping electric double layers lead to a decrease of the activation energy, while a smaller separation distance D will hinder the diffusion of the solutes. However, the dissolution process is shown to be reaction-limited rather than diffusion-limited even at 0.3 nm separation distance.[22] Studies also show that pressure up to 500 atm has very little effect on the activation energy.[26] One reservation is that our results are obtained at room temperature, and that higher temperature, which most geological samples experience, may induce more complicated relationships between dissolution, electrochemical reactions, and pressure.

The dissolution experiments presented here using the EC-SFA reveal the importance of the electrochemical surface

dx.doi.org/10.1021/jp408144g | J. Phys. Chem. B 2013, 117, 16369–16387

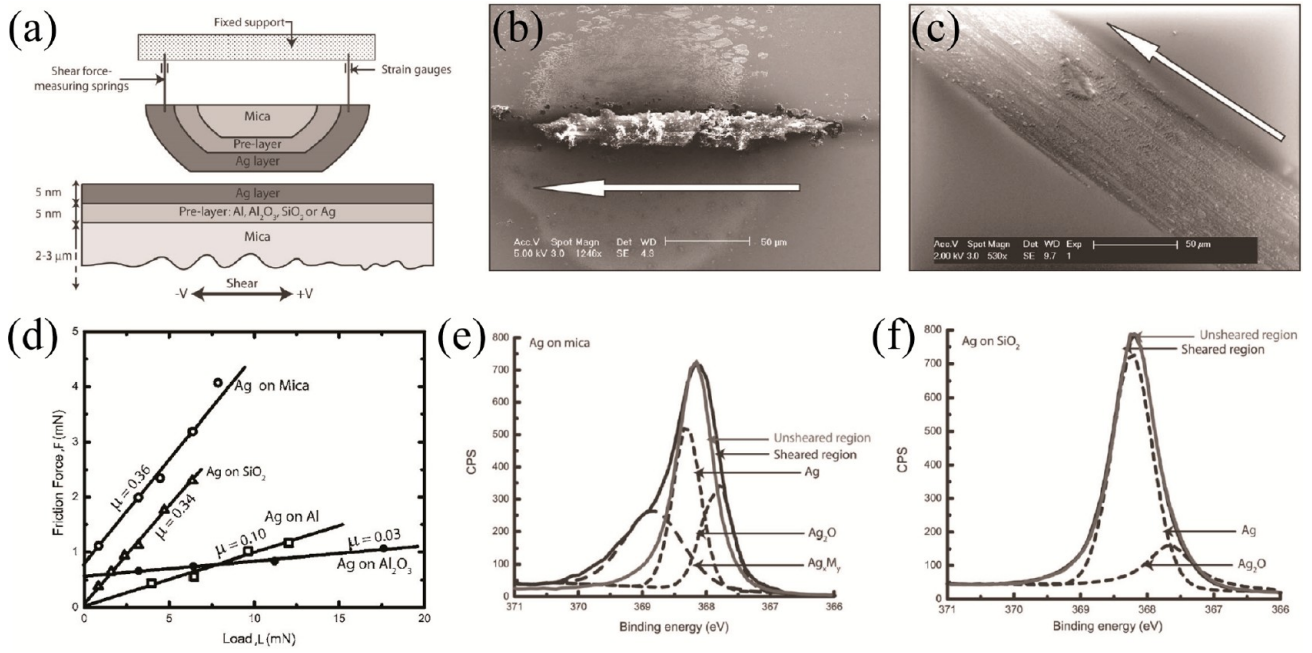

Figure 7. (a) Schematic of the surface. Atomically smooth and back-silvered mica (2−3 μm) was glued onto cylindrical silica discs using UV glue, followed by electron beam evaporation of a prelayer (SiO_2 in this case) and Ag layer with thicknesses of 5 nm. SEM image of the wear track of (b) Ag on Al and (c) Ag on SiO_2 surface formed by shearing (the white arrow shows the shearing direction). (d) Friction forces before surface damage as a function of load for various substrates. The friction coefficient μ is defined as df/dL. XPS spectra of the sheared (black) and unsheared (gray) regions of thin (e) Ag on mica and (f) Ag on SiO_2. Reprinted with permission from ref 37. Copyright 2006 AIP Publishing LLC.

potentials in the pressure solution phenomenon observed in geological samples (see Figure 2). The proposed electrochemical model is general and may provide a unifying key to understand processes important not only to geology but also to many seemingly unrelated fields, technologies, and disciplines, such as chemical mechanical polishing (CMP), micro- and nanofluidic phenomena, and corrosion.

6. TRIBOCHEMICAL REACTIONS OCCURRING AT SHEARING INTERFACES

Understanding tribochemical reactions at interfaces that move relative to each other has become important in applications of micro- and nanodevices, and further improvements require a better understanding of their fundamental mechanisms. One of the main mechanisms that can trigger chemical reactions is frictional heating. The frictional heating not only increases the average temperature of the shearing contact but significantly increases the *local* temperature (500−1000 K)[30,31] of the shearing junctions. The steep increase in local temperature can induce tribochemical reactions (i.e., oxidation) at shearing junctions[32,33] and thus alter the tribological properties compared to fresh unreacted surfaces, which can eventually impact the overall performance of the tribological devices. The chemical reactivity of the shearing surfaces strongly depends on the physical properties of the surfaces, i.e., surface morphology and physical defects.[34−36]

Akubulut and co-workers[37] used an SFA coupled with *ex situ* measurements of X-ray photoelectron spectroscopy (XPS) and scanning electron microscopy (SEM) to investigate the tribochemical/tribological properties of a thin (5−10 nm) Ag layer on various substrates (see Figure 7a for the schematics). Despite the fact that all shearing surfaces were Ag, they exhibited a different roughness depending on the substrates that they were deposited on Al_2O_3, Al, mica, and SiO_2 (rms roughness of 0.83, 1.02, 1.36, and 1.83 nm, respectively). The friction forces measured with the SFA show that the surfaces with larger roughness exhibit a higher friction coefficient ($\mu = df/dL$, see Figure 7d) below a certain level of roughness.

The structural changes/damage of the surfaces after shearing were investigated using SEM (Figure 7b and c). Initially, smooth surfaces (Figure 7b, Ag on Al, rms roughness of 1.02 nm) had very large features at the center of the contact where the pressure had been the highest, which resulted in a significant increase in roughness. Meanwhile, initially rough surfaces (Figure 7c, Ag on SiO_2, mean rms roughness of 1.83 nm) had smaller features that were distributed uniformly along the contact. Compared to the initially smooth surfaces, the initially rough surfaces have a smaller "real" contact area, which causes damage to the rough surfaces much more easily due to higher local stresses and strains. Thus, rough surfaces produce many, but small, wear debris particles, while smooth surfaces produce a few, but large, debris particles.

The chemical changes induced from shearing were studied using XPS. When the Ag was deposited on an Al_2O_3 layer and sheared with a symmetric surface, extensive oxidation was observed (relative composition of 80−85% Ag and 15−20% Ag_2O; see Figure 7e). Meanwhile, Ag deposited on SiO_2 had no apparent chemical difference between the sheared and unsheared regions only showing slight natural oxidation (5−10%) in both regions (see Figure 7f). These results suggest that the local temperature increase of Ag on SiO_2 was not enough for the oxidation reaction to take place. Furthermore, surfaces exhibiting only adhesive and therefore much higher friction (having a finite friction force at zero load, see Ag on mica and Ag on Al_2O_3) had significant changes in the surface chemistry in the sheared regions of Ag (see Figure 7e) which could be related to the complex relation among the roughness, stiffness, local temperature, and reactivity of the Ag surfaces.

dx.doi.org/10.1021/jp408144g | J. Phys. Chem. B 2013, 117, 16369−16387

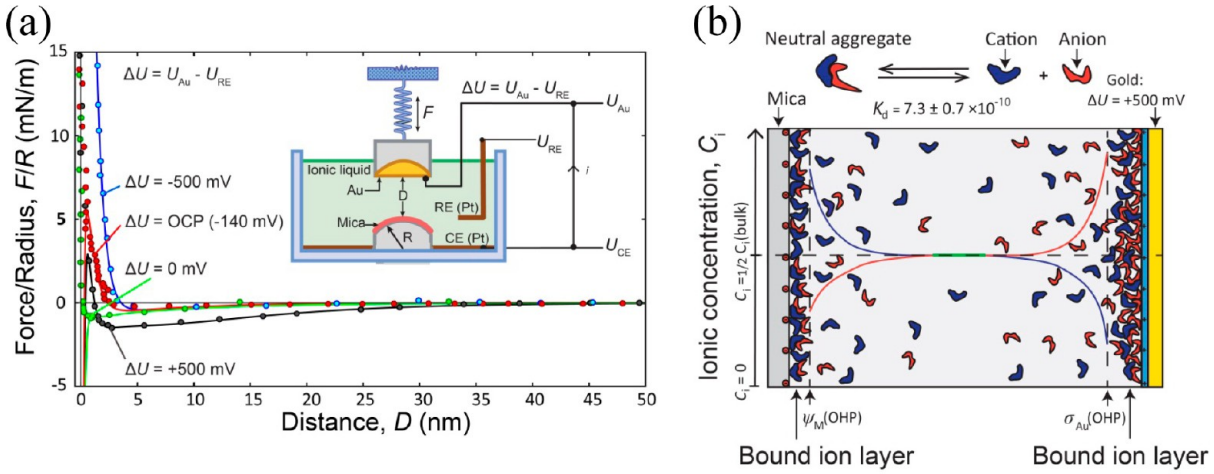

Figure 8. (a) Representative force–distance profiles measured across the ionic liquid 1-butyl-3-methylimidazolium bis(trifluoromethanesulfonyl)-imide ($[C_4mim][NTf_2]$) under electrochemical control. External potentials, ΔU, are indicated next to each curve. Points correspond to experimental data and lines to theoretical calculations using a "DLVO-type" interaction potential: DLVO superimposed with a short-range ion–surface binding term. The double layer portions of the interaction potentials were found to decay with an effective Debye length of $\kappa^{-1} = 11 \pm 2$ nm. Inset: Schematic of the EC-SFA setup employed in the measurement of forces across $[C_4mim][NTf_2]$. (b) Diagram of the diffuse electric double layers formed by the $[C_4mim][NTf_2]$ ions. Effectively dissociated ion pairs are generated via the equilibrium dissociation reaction above, where the equilibrium, and resultant effective ionic strength, depends on a balance of ion–ion interaction energies (screened by surrounding ions and accounted for via the low frequency of the bulk ionic liquid relative permittivity, ε) favoring aggregation and thermal entropic energies (Boltzmann distribution of energy states) favoring dissociation. (Adapted from ref 40. Copyright 2013 National Academy of Sciences, USA.)

7. ELECTROCHEMICALLY INDUCED DOUBLE LAYER FORCES IN IONIC LIQUIDS

Ionic liquids are receiving considerable attention as promising materials for numerous technological applications, including energy storage devices.[38] Since interfacial phenomena are a key determinant for the performance of ionic-liquid-based energy storage devices, numerous research groups, including ours, are actively involved in elucidating the interfacial behavior of ionic liquids. Of particular relevance to this review are recent works by Hayes et al.[39] that utilized AFM to study the near-surface structuring of ionic liquids at gold electrode surfaces, and our complementary work with the EC-SFA where we found that ionic liquids also form long-range diffuse electric double layers (out to 15+ nm) under certain applied potentials (Figure 8).[40]

The interfacial structuring of ionic liquids was first reported by Horn, Evans, and Ninham in 1988, when they used a SFA to study the ionic liquid ethylammonium nitrate (EAN) in an interface consisting of two mica surfaces.[41] In this symmetric setup, the force–distance profiles measured across pure EAN were found to be of short range ($D < 5$ nm) and "oscillatory" in nature, where steep repulsive barriers of increasing magnitude alternate with abrupt unstable attractive "jumps in" of 0.5–0.6 nm, on the order of the size of a cation–anion pair of EAN ions.[41] "Oscillatory" interaction profiles are indicative of layered molecular ordering by nanoconfined liquids,[42] and analogous "oscillatory" force profiles have been measured across both polar[43] and non-polar[44] liquids, where the oscillations can be superimposed with additional interaction forces, including DLVO interactions. However, Horn et al. noted that the oscillations measured across EAN do not appear to be superimposed with any additional forces.[41]

With the recent renaissance in ionic liquids research, clarifying the mechanism of electric double layer formation by ionic liquids again became a focus of numerous experimental and theoretical studies.[38] For example, Perkin and colleagues utilized a SFA to study a range of common ionic liquids confined between symmetric mica surfaces, with a particular emphasis on 1-alkyl-3-methylimidazolium bis-(trifluoromethanesulfonyl)imide ($[C_nmim][NTf_2]$) ionic liquids, where n corresponds to the number of carbons in a linear alkyl substituent.[45,46] Perkin et al.[46] found that $[C_nmim][NTf_2]$ ionic liquids with $n < 6$ exhibit "oscillatory" force–distance profiles indicative of molecular layering, where the period of the instabilities again corresponds to the size of one cation–anion pair. However, once $n \geq 6$, ionic liquids abruptly transition to "bilayer" structures with segregated ionic and non-polar domains. AFM has also been heavily utilized to study the interfacial structuring of ionic liquids,[39,47] with most, if not all, studies indicating that ionic liquids form "oscillatory" layered structures at single surfaces,[47] in agreement with X-ray reflectivity studies.[48] Notably, Hayes et al.[39] used AFM to demonstrate that the range of interfacial structuring at a gold electrode surface arising from surface-bound ions increases upon applying electrochemical biases to the surfaces.

Recently, the EC-SFA technique allowed us to measure the equilibrium interaction forces across the ionic liquid $[C_4mim][NTf_2]$, and our results demonstrate that ionic liquids can also form diffuse electric double layers at confined interfaces (Figure 8).[40] The decay length of the electrostatic interaction that we measured—the effective Debye length—is in excellent agreement with a thermodynamic model that we proposed based on the energetics of ions interacting in a dielectric medium.[40] Our results demonstrate that, outside of bound ion layers, most of the ions in ionic liquids are expected to behave as a coordinated ionic network, and are therefore not "free" to contribute to electrostatic screening. Additionally, this framework provides molecular-scale insight into tuning the chemical equilibrium between the coordinated ionic network and the effectively dissociated ions (defects within the ionic network), thus providing a strategy for controlling the ranges and strengths of electrostatic interactions in ionic liquids.[40]

This finding also provides further justification for the comparatively low ionic conductivities of ionic liquids: typical

dx.doi.org/10.1021/jp408144g | J. Phys. Chem. B 2013, 117, 16369–16387

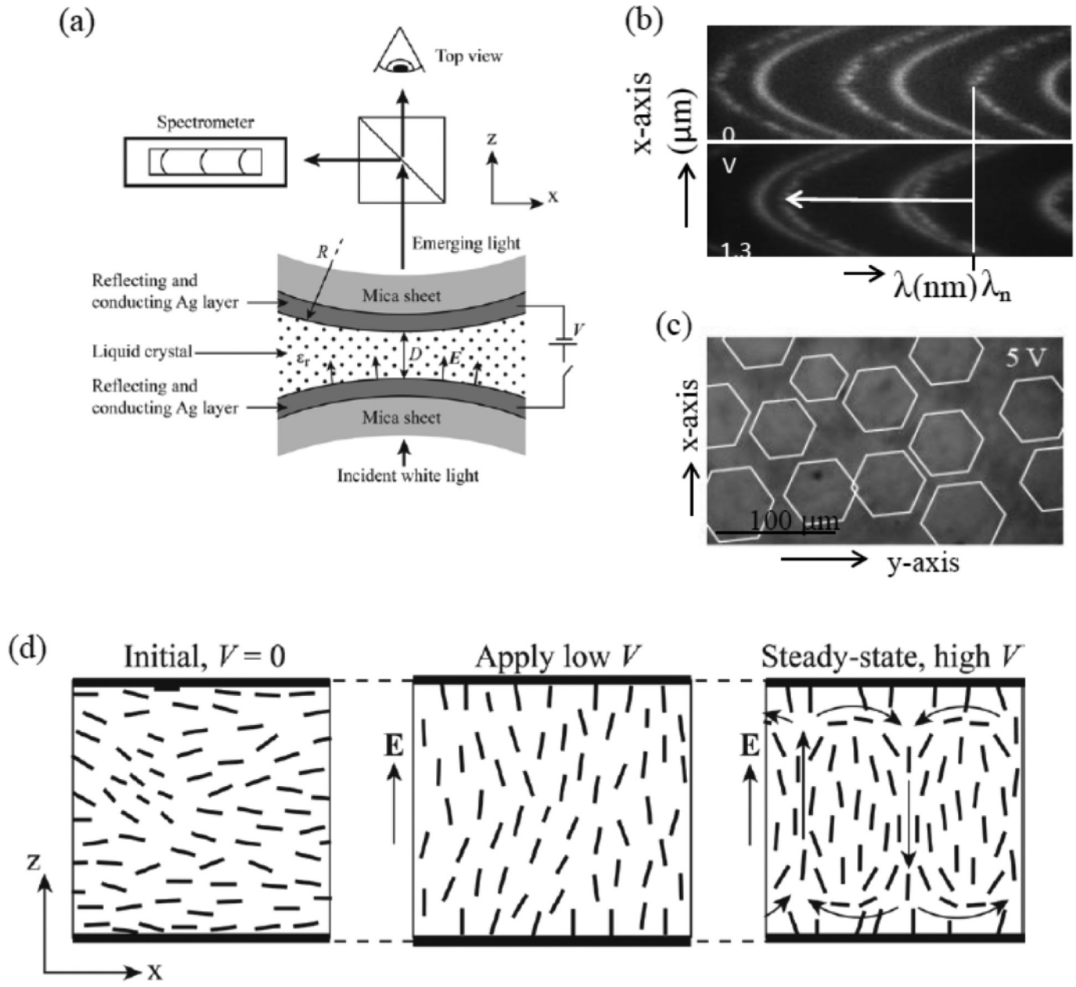

Figure 9. (a) Schematic of an electric field setup in the SFA. Two silver surfaces (55 nm thick) that are facing each other act as the electrodes, and applying a voltage across them generates an electric field across the medium between them. At 7 μm separation distances, the SFA technique gives FECO fringes with a spacing of 10−30 nm in wavelength. A beam splitter allows for simultaneous measurement of FECO fringes and the top view. (b) At no applied voltage (upper panel), the FECO fringes demonstrate the birefringent nature of the liquid crystal, since the director of the anisotropic molecule of the liquid crystal is parallel to the surfaces. The liquid crystal molecules will try to align along a weak electric field (low voltage). This can be seen on the FECO fringe as a movement of every other fringe to lower wavelengths (due to a shift to a higher refractive index value). (c) At higher electric fields (higher voltages), the splitting of the fringes due to refractive index disappears (above the Fréedericksz transition). However, the top view reveals high mobility of molecules in a hexagonal pattern (white hexagons are added as an aid for visualization), or the so-called Carr−Helfrich effect. (d) Schematic cross section showing the molecular behavior from alignment of the liquid crystal molecules along the electric field at weak electric fields (low voltage) to flow of molecules at high electric fields (higher voltage).

conductivities for aprotic ionic liquids range from 0.1 to 14 mS/cm,[49] while conventional aqueous electrolytes exhibit ionic conductivities of 500−700 mS/cm.[49] Previous studies have shown that the high viscosities of ionic liquids arise from high degrees of ionic coordination within the bulk ionic liquids, and high viscosities correspondingly slow the diffusion of ions.[50] Our work shows that the high degree of ionic coordination present in ionic liquids also substantially reduces the (instantaneous) population of effectively dissociated ions that are available to diffuse independently of the surrounding ionic network.[40]

Our results differ from previous SFA and AFM measurements that found only short-range oscillatory forces,[39,41,45−47] because the gold electrode surfaces utilized in our EC-SFA setup are molecularly smooth (0.2 RMS roughness) but polycrystalline, which suppresses or smears out the oscillatory layering of the $[C_4mim][NTf_2]$ ions.[40,51] Additionally, the presence (or absence) of long-range electrostatic effects was found to depend on specific ion−surface chemical interactions, where the $[NTf_2]$ anions did not entirely screen the positive gold surfaces via bound ion layers, resulting in long-range double layer interactions.[40] This observation is consistent with a recent neutron scattering study by Lauw et al.[52] of the interfacial structure of a $[NTf_2]$-based ionic liquid at gold electrodes, where the surface-bound ion layers were found to be enriched in cations, even under positive electrochemical biases. Lauw et al.[52] also raised the possibility that "oscillatory" force measurements across ionic liquids may be primarily related to packing constraints arising from the arrangement of large ionic liquid ions at solid−liquid interfaces (like liquid molecules), as opposed to being indicative of changes in the relative distributions of cation and anion densities next to charged surfaces (i.e., electrostatic screening).

dx.doi.org/10.1021/jp408144g | J. Phys. Chem. B 2013, 117, 16369−16387

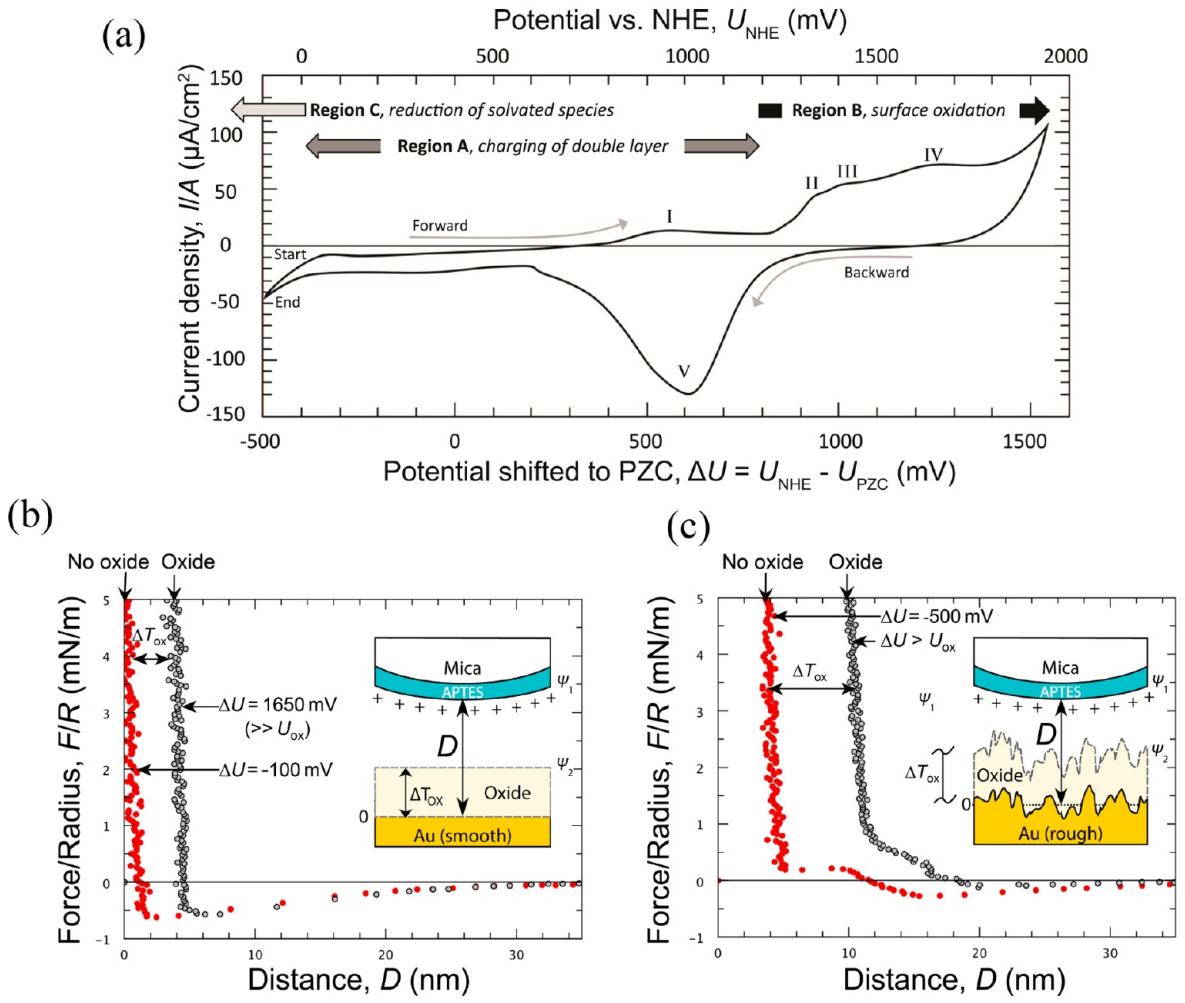

Figure 10. (a) Typical cyclic voltamogram (CV) of a typical gold electrode recorded with a linear sweep rate of 50 mV/s in 1 mM HNO_3 at pH 3 using the newly developed EC-SFA setup shown in Figure 3a. (b) Typical force−distance profiles measured during approach of the gold and APTES coated mica surfaces measured at high (anodic) externally applied electrochemical potentials that are higher than the oxidation potential, U_{OX}, where the gold surface oxidizes ($\Delta U \gg U_{OX}$) of the smooth gold surface Au, and (c) the electrochemically roughened gold surface. (Adapted from ref 11.)

8. ELECTRIC FIELD EFFECTS ON THIN LIQUID CRYSTAL FILMS

The SFA with an electric cell can shed light on the interplay between interaction forces, polarization, molecular rotation, and flow of a nematic liquid crystal in an external electric field. A liquid crystal consists of anisotropic polar molecules, where as a medium it has some degree of crystalline order, yet is liquid-like in at least one direction.[53] For example, a nematic liquid crystal has correlations along the preferred direction (the so-called "director") that are not equivalent (i.e., anisotropic) to those along the two perpendicular directions. Their anisotropic nature often makes them highly birefringent materials, which makes them widely used in optical devices as thin films between two electrodes, which provides the ability to manipulate polarized background light. Nematic liquid crystals can easily flow or rotate and respond fast to an external electric or magnetic field; however, the flows of nematics are more complex than those of isotropic liquids, since there is a complex coupling between the translational and orientational motions of the molecules.[53] Two of the main issues with complex flow are that the flow of the molecules affects the alignment of the molecules and that a change in the alignment can induce a flow.

Figure 9a shows an experimental SFA setup for studying electric field effects on a liquid crystal medium. This electric cell generates an electric field between two surfaces but does not polarize the surfaces in the same way as the setup shown in Figure 3. The liquid crystal is trapped between two reflective silver electrodes where the light that passes through the electrodes is divided by a beam splitter that allows for simultaneous distance and polarization measurements using the SFA-FECO optical techniques, as well as monitoring refractive index fluctuations by viewing the top surface of the liquid crystal using an optical microscope.

The liquid crystal studied here is the commonly used 4′-*n*-pentyl-4-cyanobiphenyl (also called 5CB), which is nematic at room temperature. The 5CB has a preferred alignment of the director parallel to a silver surface. Its nematic structure can easily be seen as the birefringent pattern in the FECO images, as seen in the upper panel of Figure 8b (separation distance of 7 μm). The refractive index parallel to the director (extraordinary wave) is higher than perpendicular to the director (ordinary wave). Also, the FECO fringes of the extraordinary waves appear rougher than those from the ordinary waves which reflects the molecular motion of the

dx.doi.org/10.1021/jp408144g | J. Phys. Chem. B 2013, 117, 16369−16387

nematic along the director. However, from the top view, the nematic appears as a uniform medium.

In an electric field, E, the molecules of 5CB (in the $x-y$ plane) will try to align the director parallel to the field. This change of alignment of the molecules changes the refractive index of the extraordinary wave in the $x-y$ plane of the surfaces to a lower value. This shift in refractive index can easily be seen in the FECO fringes as the extraordinary wave moves to the left (closer to the fringes of the ordinary wave). Figure 9b shows how light polarized along the director changed the wavelength in the FECO image from going from no applied voltage to 1.3 V. Interestingly, the FECO fringes of the ordinary wave do not display any changes, which means that there is no detectable change in the separation distance between the surfaces. Above 2.5 V, the extraordinary wave overlaps with the ordinary wave, and upon removal of the applied voltage, the fringes of the extraordinary waves do not relax back to the initial alignment parallel to the silver surface (at least not coherently). This is the so-called Fréedericksz transition[54] (the voltage is independent of the sample thickness), which is a second order phase transition of the alignment of the director as it approaches parallel to the external electric field.

Close to and above the Fréedericksz transition voltage, the top view starts to show dynamic distortions in the liquid crystal due to fluctuating changes in the refractive index. Figure 9c shows that, in even higher electric fields (here 5 V), regular hexagonal patterns form of fluctuating regions with different refractive index in the center of the hexagons compared to the edges. These fluctuating regions are due to convective flow instabilities, or the so-called Carr–Helfrich effect[53,55]—where the flow is driven by a combination of electrostatic torque and hydrodynamic torques. The flow pattern shares some similarities with the Bénard cell phenomenon, and is schematically drawn in Figure 9d, right panel. However, with the EC SFA setup, we only performed experiments under applied electric fields of up to 20 V, which should still be too low to enter the turbulent regime.[51]

Previous SFA experiments have provided interesting results on intersurface forces (both normal and frictional forces) of liquid crystals between two mica surfaces.[56] Other techniques, like the QCM-D with an electrochemical cell, have shown interesting electroviscous effects of 5CB near a surface.[57] We have also measured the forces exerted on the surfaces in an electric field and successfully correlated these measurements with the flow patterns.

9. CHEMICAL REACTIONS—DISSOLUTION, ADSORPTION (GROWTH), OXIDATION, AND REDUCTION

Due to the angstrom distance resolution and the possibility of stable (equilibrium) measurements over long time durations, the SFA technique can be used to study in situ the dissolution of materials (e.g., pressure solution, see section 4) as well as the growth and/or adsorption of atomically thin films at interfaces. Recently, it was demonstrated that the EC-SFA allows for simultaneous growth of a passivating oxide film *and* the identification of the chemical nature of the thin growing oxide film in situ.[11] Figure 10a shows a typical cyclic voltamogram (CV) with characteristic features of an amorphous and atomically smooth Au surface measured in the EC-SFA. The potential axis shows the applied potential with respect to U_{NHE} (potential of a "normal hydrogen electrode", $U_{NHE} = U + 197$ mV), which is commonly used in electrochemistry. However, in electrochemical surface science, it is more convenient to use a scale that refers to the potential of zero charge, U_{PZC}, i.e., the electrochemically applied potential at which the surface charge on the working electrode is zero ($\Delta U = U_{NHE} + U_{PZC}$). A potential sweep in the form of a triangular wave was imposed on the Au surface between $\Delta U = 1500$ and -500 mV at a rate of 50 mV/s.

The CV in Figure 10a displays three distinct regions, viz., regions A, B, and C, and five peaks, that are characteristic for a well-prepared gold surface. Region A shows the current associated with the charging of the electric double layer due to specific adsorption of ions onto the Au electrode surface. Peak I in this region corresponds to the chemisorption of nitrate and hydroxide ions onto the electrode from the solution. The surface oxidation of Au is demonstrated in region B and results in the flow of a faradaic current through the electrochemical interface. The oxidation peaks II, III, and IV in region B are associated with the formation of a passivating oxide layer of Au_nO_m on the Au surface and has important implications about the mechanism of oxide film formation.[58,59] On reversing the applied potential to the oxidized Au surface, it gets reduced back to Au at a potential of 1025 mV vs NHE. Region C shows the reduction of the solvated protons and oxygen at the Au surface.

Parts b and c of Figure 10 show the interaction forces measured between an oxidized Au electrode surface (gray circles; for atomically smooth and electrochemically roughened surfaces, respectively) and a positively charged APTES coated molecularly smooth mica in 1 mM HNO_3 solution at pH 3 (ψ_1 = +55 mV), as well as the thickness of the grown gold oxide Au_nO_m layer, using the EC-SFA. The passive layer of gold oxide was grown on the electrode surface by polarizing the gold electrodes above the oxidation potential, ΔU_{ox}.

The force–distance profiles with the gold oxide surfaces (gray circles) show long-range attractive double layer forces, similar to a gold surface (without oxide layer) at negative potentials apposing the same APTES surface (red circles in Figure 10b,c), instead of the repulsive double layer forces that would be anticipated for a positively charged surface (see Figure 3). The observation of long-ranged attractive double layer forces indicates that the oxide surface fully screens the positive electrochemical potential applied to the underlying (unoxidized) gold electrode surfaces. The resultant negative surface potential observed for the gold oxide surface (surface potential $\psi_2 = -25$ mV) is attributed to the specific adsorption of a layer of hydroxide ions on the oxide surface. Further, the agreement between the ranges and magnitudes of the measured double layer forces for the reduced gold surface at $\Delta U = -100$ mV and oxidized gold electrode surface at $\Delta U = 1650$ mV is due to similar surface potential: the reduced gold surface exhibits a negative surface potential of $\psi_2 = -25$ mV due to negative surface charging induced by the application of negative electrochemical potentials.

The EC-SFA also provides a direct measurement of the in situ oxide layer thickness and oxide thin-film chemistry. The chemical composition of the oxide layer can be determined from the thickness of the oxide layer (directly measured in the EC-SFA) and the surface charge on the electrode. The two most probable electrochemical oxidation reactions of the Au surface are

Electrochemical reaction 1:

$$2Au + 3H_2O \rightarrow Au_2O_3 + 6e^- + 6H^+$$

dx.doi.org/10.1021/jp408144g | J. Phys. Chem. B 2013, 117, 16369–16387

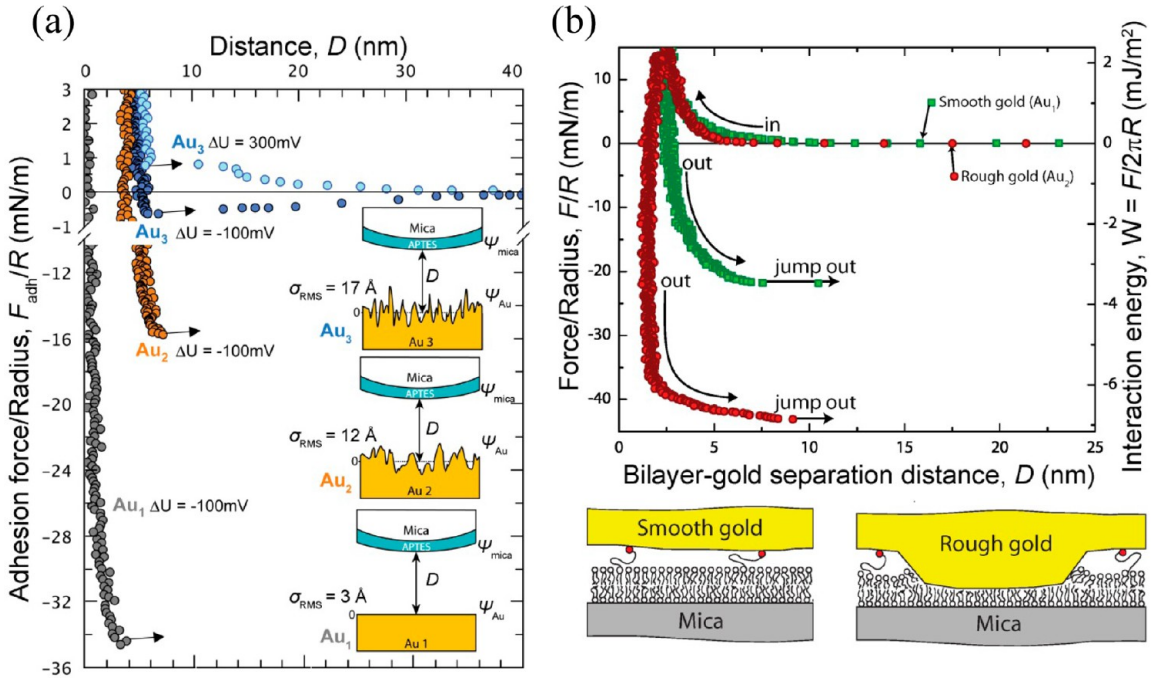

Figure 11. Two examples of systems in which the adhesion is modulated by controlling the electrochemical potential and/or the surface roughness of a gold surface. In part a, the adhesion is measured between gold surfaces and the positively charged APTES-coated mica surfaces. As the surface roughness of the gold increases, the adhesion between the surfaces decreases. (Adapted from ref 11.) In part b, adhesion is measured between an amine-terminated PEGolated lipid bilayer and an apposing gold surface. Increasing the surface roughness of the gold now leads to much larger adhesion. These two examples illustrate the difference of adhesion of a gold surface of varying roughness with both hard and soft surfaces: For hard surfaces (mica), as the surface roughness increases, the contact area between the surfaces dramatically decreases, leading to decreased adhesion. Conversely, for soft surfaces (lipid bilayer), asperities on the rough gold surface penetrate into the bilayer, leading to greater adhesion due to the increased contact area and, possibly, hydrophobic interactions. The red data points are for a bare (not oxidized) gold at a surface potential similar to the oxide gold surface, and are shown for comparison. (Adapted from ref 62. Reproduced with permission from The Royal Society of Chemistry.)

Electrochemical reaction 2

$$Au + 3H_2O \rightarrow Au(OH)_3 + 3e^- + 3H^+$$

The calculated thickness of the oxide layer can be estimated using Faraday's law of electrolysis together with the measured charge density consumed by the gold electrode.[11] For the above example, the calculated thicknesses of an oxide layer grown on atomically smooth gold were 9.4 and 31.4 Å for reactions 1 and 2, respectively. Compared with the measured thickness of ΔT_{ox} = 32.7 ± 3.3 Å using the EC-SFA (see Figure 10b), this allowed us to conclude that electrochemical reaction 2 with oxide layer $Au(OH)_3$ is the correct reaction, which is also consistent with previous work by several authors[58,60] as well as the calculated Pourbaix diagram for gold.[61]

The thickness of the gold oxide grown on an electrochemically roughened (by applying oxidation−reduction cyclic voltamograms from −200 mV vs Ag|AgCl to +1400 mV vs Ag|AgCl at a high rate of 3 V/s) Au electrode surface was about 60 Å, which is twice the value expected assuming a homogeneous $Au(OH)_3$ oxide layer. This may be attributed to the rapid growth of the oxide layer on the rough Au surface where the electric field intensities are higher on asperities, compared to a molecularly smooth surface, or that the film is less dense.

The ability to measure the oxidation current simultaneously with the thickness of a growing oxide film allows determination of the chemistry of oxide films in situ, a capability which is unique compared to other electrochemical techniques.

10. ADHESION AND FRICTION—EFFECTS OF ELECTRIC FIELDS

Both the adhesion and friction between surfaces can be modulated using the EC-SFA by controlling the electrochemical potential ΔU at an interface. By controllably adjusting ΔU at a gold surface, the electrostatic OHP potential ψ_{Au} can be affected, which can affect the range and magnitude of the electrostatic double layer forces, as discussed in sections 2, 3, and 5. Another way to influence the adhesion and friction is by altering the actual surface structure by performing the electrochemical reactions discussed in section 9. Surface restructuring can be induced by repeated oxidation and reduction of the gold surface, resulting in progressive roughening of the surface. The effects of adjusting ΔU and subsequent effects on ψ have been discussed fully earlier in this review.[5,6,11] We examine in this section the effect of surface restructuring of a gold surface on the adhesion and friction forces between the gold surface and an apposing mica surface of varying functionality.

The adhesive interactions between a gold surface under electrochemical control and a mica surface functionalized with a monolayer of APTES were previously examined in detail.[11] As shown in Figure 11a, the adhesion decreases dramatically as the surface roughness on the gold surface increases (Au-1 to Au-3). In this case, the large decrease in adhesion is a result of the decreased contact area between the interfaces. For identical surface potentials, the adhesion decreases dramatically the rougher the surfaces. Asperities in the contact zone result in less area of contact, and this can also be observed from the shapes

dx.doi.org/10.1021/jp408144g | J. Phys. Chem. B 2013, 117, 16369−16387

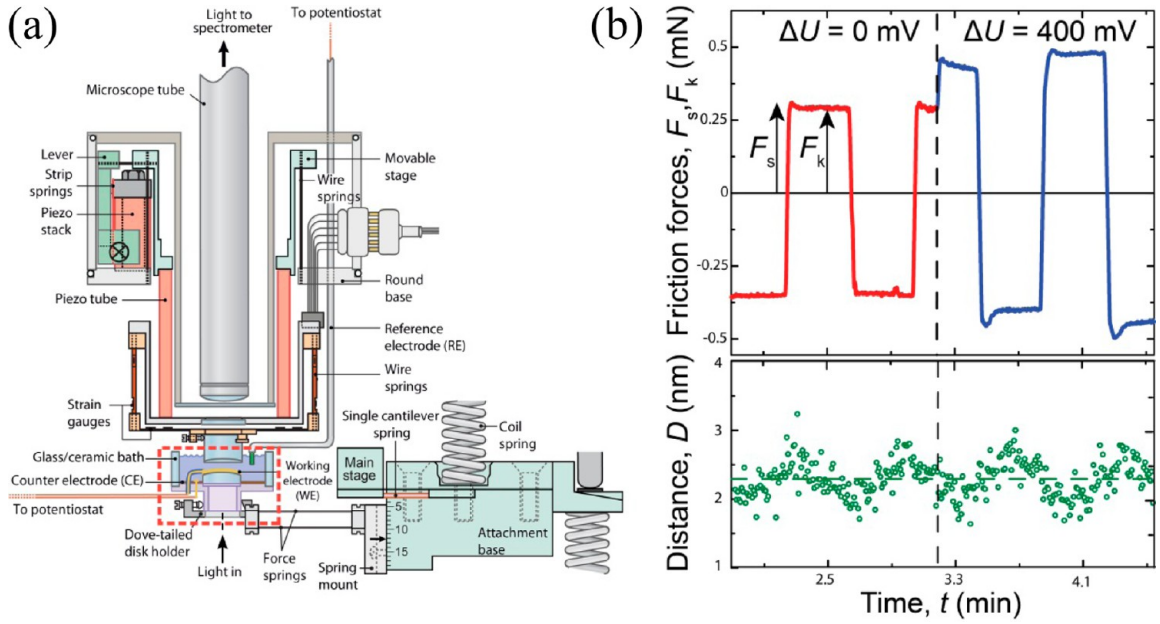

Figure 12. (a) Schematic representation of the 3D sensor actuator mounted with the electrochemical cell. (b) Upper panel: frictional forces measured during reciprocal sliding of a mica surface against a gold electrode at 500 nm/s under a normal load of 1.7 mN. During the sliding plateau, the surface potential of the gold electrode was increased from 0 to 400 mV while monitoring the friction force and surface separation (lower panel). (Adapted from ref 11.)

of the FECO fringes, confirming non-adhesive contact mechanics for the Au-2 and Au-3 rough surfaces, as compared to the molecularly smooth Au-1 surface.

In a similar experiment, a mica surface was functionalized with a PEGolated lipid bilayer and the interactions were measured with both smooth (Au-1) and rough (Au-2) gold surfaces.[62] For the bilayer, the adhesion actually increases for the rough surface, as shown in Figure 11b. Asperities induce large local pressures at the bilayer interface, and as additional force is applied, the asperities are able to puncture through the bilayer interface. This puncturing results in an increased contact area of the gold surface with the hydrophobic bilayer interior, causing the adhesion energy to roughly double as compared to the smooth surface.

These two examples illustrate a fundamental difference of the effects of surface restructuring when interacting with a hard or soft surface. A hard surface interacting with a rough surface results in less contact area than with a smooth surface of the same material, and thus smaller adhesion. A soft surface interacting with a rough surface, on the other hand, can result in asperity breakthrough into the soft surface, leading to increased adhesion.[62]

Electrochemical control of the surface potential can also modify the properties of a confined fluid. A clear manifestation of such a phenomenon can be observed when the fluid is sheared between two flat surfaces such as mica. To perform such an experiment, Valtiner et al.[11] modified a recently developed 3D sensor actuator[8] and installed it with an electrochemical cell in the SFA (Figure 12a). In this new setup, the Ag/AgCl reference electrode was inserted through the actuator and its extremity was immersed in a small bath of electrolyte solution. The working electrode was a gold surface immersed in the same electrolyte solution. The counter electrode was deposited at the bottom of the bath ensuring extensive contact with the electrolyte solution. The upper surface (bare mica) was actuated with a linear, laterally reciprocating sliding motion, and the frictional forces and separation distances between the mica surface and the gold electrode were recorded simultaneously.

The results, shown in Figure 12b, are an example of the evolution of the friction force as a function of time (friction trace). During the sliding of the mica surface, the separation distance was found to oscillate slightly between 2 and 3 nm. These oscillations were in phase with the frequency of the reciprocal motion. The frictional forces measured at constant sliding speed and applied normal load were found to be strongly dependent on the applied electrochemical potential to the gold surface. In Figure 12b, the electrochemical potential was abruptly changed from 0 to 400 mV during the sliding plateau of the mica surface. Immediately after this change in potential, the friction force increased by almost 50% with the appearance of stiction spikes after a few back and forth sliding cycles. The authors ascribed this change in frictional forces to an electroviscous effect. They found that, upon increasing the surface potential, the viscosity of the highly confined fluid, which was 5 orders of magnitude higher than the bulk water viscosity, increased from 190 to 250 Pa·s.

These experiments suggest new ways to study such complex dynamic phenomena by combining different measurement techniques such as optical microscopy, SFA, and electrochemical potential and current measurements in order to gain more insights into their chemical−physical origins.

11. FUTURE WORKS

The electrochemical attachment to the SFA could easily be adapted to other surface characterization techniques involving microscopic or spectroscopic imaging or measurements, both in vapor (vacuum) and liquids, such as IR, X-ray, SHG, SFG, and SANS.

Redox-Dependent Interaction Forces between Protein Surfaces. So far, the EC-SFA has been used to measure and control the intersurface forces—while controlling the

dx.doi.org/10.1021/jp408144g | J. Phys. Chem. B 2013, 117, 16369−16387

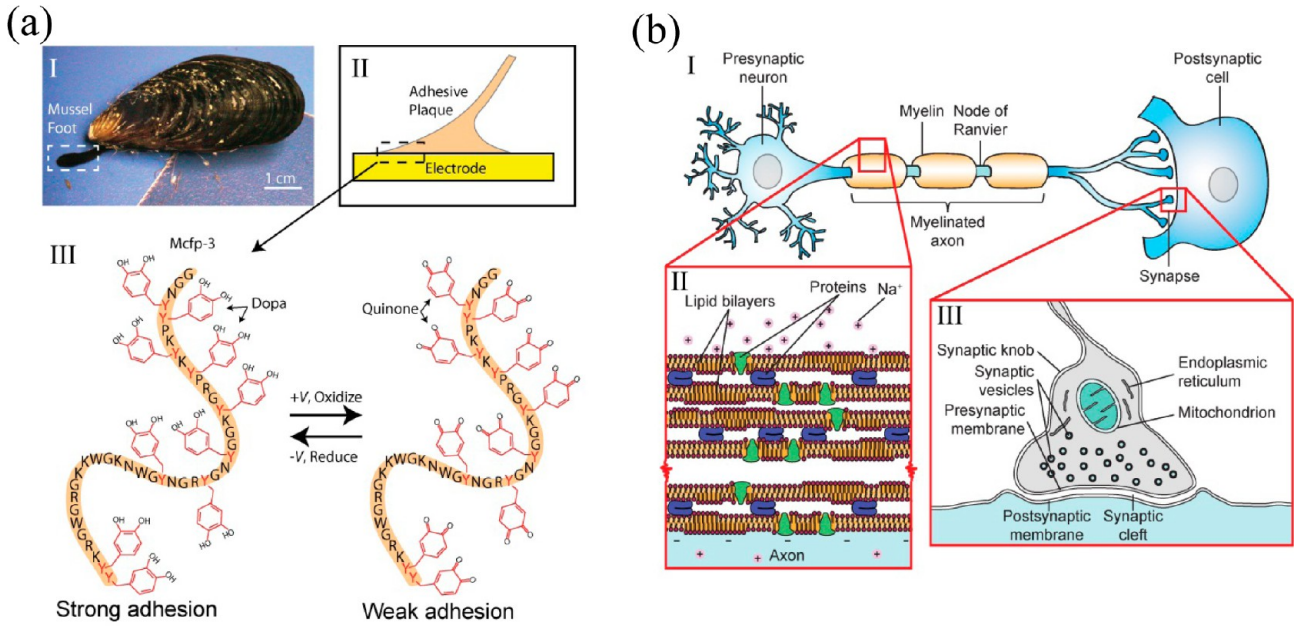

Figure 13. (a) A redox-dependent adhesive protein. (I) An adult California mussel (*Mytilus californianus*) is shown as its foot (contained by the white dashed box) extending to form a new surface adhesive plaque. (II) A schematic of a mussel adhesive plaque. The adhesive proteins in the plaque are redox sensitive, and they may be oxidized or reduced by an electrode surface. (III) The *Mytilus californianus* foot protein-3 (Mcfp-3). The amino acid Dopa may be oxidized or reduced with electric potential, *V*, to inhibit or promote adhesion, respectively. (b) Schematic of a neuron. (I) The general structure of the primary components, including the presynaptic neuron, the axon, and the postsynaptic cell. (II) The structure of myelin, which consists of multiple bilayers that incorporate various proteins. (III) The structure of a synapse, which is responsible for cellular communication via neurotransmitters.

electrochemical potential of one surface—between inorganic surfaces (metals, oxides, or minerals) in aqueous or synthetic liquid solutions (ionic liquids or liquid crystals), as well as studying electrochemical reactions at inorganic surfaces. In the future, we believe that the EC-SFA can be a powerful tool for analyzing the subtle electrochemical (redox)-dependent interactions that occur at biological interfaces or between biomolecules, a notable example of which can be seen in the adhesive behavior of mussel foot proteins (mfp's). In its natural marine habitat, a mussel's foot (Figure 13a-I) will secrete a protein-based adhesive glue that strongly adheres to organic and inorganic wet surfaces, allowing the mussel to tether to surfaces underwater.[63] The unique proteins that comprise the adhesive plaque contain a high density of the rare amino acid 3,4-dihydroxyphenylalanine (Dopa), which has been shown to mediate the plaque's adhesion to inorganic surfaces through bidentate hydrogen bonds or coordination bonds that form via Dopa's cathechol arms.[64,65] Dopa has been successfully used as an adhesive agent in mussel-inspired adhesives;[66−68] however, to the detriment of its adhesive potential, Dopa oxidizes (to dopaquinone) at physiological pH, which presents a significant obstacle to many practical applications of mussel-inspired adhesives.[69,70] With the EC-SFA, we can apply oxidizing and reducing potentials, *V*, at a mfp-adsorbed electrode surface to control the redox state of mfp's, *in situ* (Figure 13a-II and III), and measure the corresponding changes in the protein conformation (film thickness) and adhesion between the mfp-adsorbed electrode surface and an apposing (organic or inorganic) surface. By correlating the redox state of surface-bound proteins with the measured interactions between a protein interface and another surface (organic, inorganic, or biomimetic surface), we can broaden our understanding of the desirable criteria that go into the design of functional protein-based devices—such as mussel-inspired adhesives, bioelectronic devices,[71,72] and biosensors.[73]

Electrochemical Potential in the Nervous System. Electrochemical potential gradients frequently occur at or across membranes in cellular systems, such as in oxidative phosphorylation that occurs at the mitochondrial inner membrane, or in the axons of neurons in the nervous system. The action potential—the electrochemical potential that is generated and transmitted through the nervous system—is responsible for directing and responding to stimuli that control the activities of all vital systems, such as the visual, sensory, and muscular systems.

In healthy tissues, an action potential can propagate through the neuron with minimum dissipation. Figure 13b-I shows a schematic of a neuron that is the primary component of the nervous system. The neuron consists of three parts—a presynaptic neuron, a (myelinated) axon, and a postsynaptic cell—where the stability of the myelin sheet is an important factor for the action potential to transmit efficiently (faster and less energy) by saltatory propagation.

Figure 13b-II shows a schematic of the compact multilamellar structure of myelin that is responsible for the electrical and ionic insulation of the axon. Disruption or swelling of the myelin structure results in sensory and motor disabilities, which is a typical sign of neurological conditions like multiple sclerosis (MS). Previous studies showed that small changes in the morphology and composition of the myelin sheet (e.g., the presence of proteins such as myelin basic protein and the lipid composition) are responsible for the stability of the myelin structure.[74−76] The EC-SFA can be used to study in detail and at the molecular scale the response of an electric potential (equivalent to an action potential) at the myelin interface while measuring the insulation properties of the myelin in real time.

dx.doi.org/10.1021/jp408144g | J. Phys. Chem. B 2013, 117, 16369−16387

The arrival of an action potential to a synapse causes the release of chemicals (see Figure 13b-III), called neurotransmitters, which are typically packed in synaptic vesicles (diameter ~40 nm). Neurotransmitter release is regulated by voltage-dependent calcium channels. Several of the notable steps in this neurotransmission process are (i) the loading of neurotransmitters into the synaptic vesicles, (ii) the docking of vesicles near the release sites, and (iii) synaptic vesicle fusion. Despite significant attention from biophysicists over several years,[77−79] the molecular mechanisms of these important events are still unclear. Using the EC-SFA, it may be possible to mimic these events, at least partially, by measuring the adhesion and separation distance between membranes and vesicles under an applied electric potential as it simulates and transmits action potentials.

■ CONCLUDING REMARKS

The electrochemical attachment to the SFA complements similar chemical probes, such as those used in atomic force microscopes (AFMs) and scanning probe microscopes (SPMs) that study much smaller, essentially nanoscale, areas, as opposed to the extended (micrometer to millimeter) surfaces of the SFA. Many interactions and chemical reactions can depend critically on the size or area of the "sample" being investigated, so that these different types of measurements complement each other. The SFA technique, however, when used with the multiple beam interferometric (MBI-FECO) optical imaging technique also allows measurements of the exact shapes, contact areas, and absolute surface separations of the interacting surfaces as well as slow relaxation or equilibration dynamics which are generally needed for fully and quantitatively analyzing or modeling the results.

■ ASSOCIATED CONTENT

Supporting Information

Photomicrograph (crossed nicols) of detrital muscovite that links quartz grains in flexible sandstone (var. itacolumite). This material is available free of charge via the Internet at http://pubs.acs.org.

■ AUTHOR INFORMATION

Corresponding Author

*Address: Chemical Engineering, M/C 5080 University of California, Santa Barbara, CA 93106-5080, USA. Phone: 805 893 8407. E-mail: Jacob@engr.ucsb.edu.

Notes

The authors declare no competing financial interest.

Biographies

Jacob N. Israelachvili received his B.A. and M.A. in (Experimental) Physics from the University of Cambridge, England, and also carried out graduate and postgraduate research work there at the Surface Physics Department of the Cavendish Laboratory. He received his Ph.D. in 1972. After a two-year EMBO research fellowship at the University of Stockholm, he left for Australia where, from 1974 to 1986, he lead an experimental research group devoted to measuring the forces between surfaces. In 1986, he joined the faculty at UCSB where he holds joint appointments as Professor in the Chemical Engineering Department, the Materials Department, and the BioMolecular Science and Engineering program. Israelachvili's research interests are in the general area of intermolecular and intersurface forces in biological, complex fluid and materials systems. He uses the surface forces apparatus for directly measuring the forces between surfaces in liquids and vapors, and for studying other interfacial phenomena at the molecular level.

Kai Kristiansen is an assistant project scientist in the field of interfacial science and soft condensed matter physics at the University of California, Santa Barbara. He received his doctor scientiarum (Dr. Scient.) from University of Oslo, Norway, in 2005 on the studies of colloidal dynamics in magnetoviscous fluids and on particle sedimentation (both experiments and computer simulations). For his postdoctoral research, he conducts and leads research using the surface forces apparatus involving friction, adhesion, and interfacial science experiments in a broad range of fields including biophysics, geophysics, colloidal science, condensed matter physics, tribology, and nanoscience, as well as develops new research instrumentation for interfacial force measurements.

Matthew A. Gebbie received his B.S. in Chemical Engineering from NC State University in 2010, where he engaged in research on the physical properties of ionic liquids in the laboratory of Prof. Wesley Henderson. He is currently a fourth year Ph.D. candidate in the Materials Department at UC Santa Barbara, where he is a member of Jacob Israelachvili's interfacial sciences research group. His research primarily focuses on understanding the interplay of interfacial forces and electrochemical potentials in confined soft matter systems, including ionic liquids and redox- and surface-active peptides.

Dong Woog Lee received his B.S. in Chemical Engineering from KAIST, South Korea, in 2008, where he worked in the biosensor laboratory of Prof. Hyun Gyu Park as an undergraduate research assistant, specifically working on electrochemical DNA sensors. He is currently a fifth year Ph.D. student in Department of Chemical Engineering at UC Santa Barbara under Prof. Jacob Israelachvili. His research focuses on studying various interaction forces in bioadhesion (membrane, proteins, biomimetic polymers) and biolubrication (articular joints, model surfaces) using the surface forces apparatus (SFA).

Stephen H. Donaldson, Jr., grew up in Pittsburgh, PA, and received his B.S. in Chemical Engineering at Virginia Tech. He is currently a Ph.D. candidate in the Department of Chemical Engineering at UC Santa Barbara working with Dr. Jacob Israelachvili and Dr. Bradley Chmelka. His thesis research focuses on elucidating the effects of hydrophobic and hydration interactions in self-assembling systems, including surfactant micelles, lipid bilayer membranes, polymers, and nanoparticles.

Saurabh Das received his Bachelor in Chemical Engineering from University Institute of Chemical Technology, Mumbai, in 2009. He is currently a fourth year Ph.D. student in the Department of Chemical Engineering at UC Santa Barbara under Prof. Jacob Israelachvili. He works on the adhesive and tribological properties of wet and dry interfaces with focus on biolubrication (conferred by proteins and polysaccharides), mussel protein adhesives, and gecko mimetic structures.

Michael V. Rapp received his B.S. in Chemical Engineering from Virginia Tech in 2011, where he worked in the surface chemistry laboratory of Prof. William Ducker. He is currently a Ph.D. student at the University of California—Santa Barbara and a NSF Graduate Research Fellow in Prof. Jacob Israelachvili's group. In his research, Michael primarily uses the SFA and AFM techniques to study hydrophobic/hydrophilic interactions, surfactant self-assembly, and wet bioadhesion.

Xavier Banquy received his M.Sc. in chemical engineering from Ecole Nationale Superieure des Industries Chimiques de Nancy, France, in 1998. He obtained his PhD in Pharmaceutical Sciences in 2009 under

the supervision of Pr Suzanne Giasson at the University of Montreral and joined Prof. Israelachvili's group at the University of California, Santa Barbara, as a post doctoral fellow. He is currently assistant Professor at the faculty of pharmacy of the University of Montreal. His current research interests are focused on the development of structured biomaterials and surfaces for the treatment of degenerative diseases such as multiple sclerosis and osteoarthritis.

Markus Valtiner received his M.Sc. (2005) and Ph.D. (2008) from Vienna University of Technology. During his Ph.D., he was awarded with the Otto Hahn medal of the Max-Planck Society while working in the department of Prof. Martin Stratmann at the Max Planck Institut für Eisenforschung. From 2009 to 2012, he was postdoctoral and Marie Curie international outgoing fellow working with Prof. Jacob Israelachvili at UC Santa Barbara. Currently, he is group leader at the Max Planck Institut für Eisenforschung working on chemistry and forces at electrochemical interfaces, single molecule force spectroscopy, and protein materials.

Jing Yu received his Ph.D. from the Department of Chemical Engineering at University of California, Santa Barbara, in 2012, where he worked in Professor Jacob Israelachvili's group. His Ph.D. research mostly focused on studying the adhesion mechanism of mussel adhesive proteins, the adhesion and friction of structured and rough surfaces, and the lubrication mechanism of human joints. He is currently a postdoctoral scholar in the Chemistry Department at California Institute of Technology.

■ ACKNOWLEDGMENTS

This research was supported by the Department of Energy, Office of Basic Energy Sciences, Division of Materials Sciences and Engineering, under Award DE-FG02-87ER-45331 (development of the SFA and electrochemical attachment, and the normal, adhesion, and lateral, friction force measurements); the National Science Foundation NSF grant CHE-1059108; partially supported by the MRSEC Program of the National Science Foundation under Award No. DMR 1121053, and also sponsored by the UCSB Institute for Collaborative Biotechnologies Grant W911NF-09-D-000 from the U.S. Army Research Office (the content of the information does not necessarily reflect the position or the policy of the Government, and no official endorsement should be inferred).

■ REFERENCES

(1) Verwey, E. J. W.; Overbeek, J. T. G. *Theory of the Stability of Lyophobic Colloids*; Elsevier: Amsterdam, The Netherlands, 1948.
(2) Israelachvili, J. N. *Intermolecular and Surface Forces*, 3rd ed.; Academic Press and Elsevier: Amsterdam, The Netherlands, 2011.
(3) Frechette, J.; Vanderlick, T. K. Double Layer Forces over Large Potential Ranges as Measured in an Electrochemical Surface Forces Apparatus. *Langmuir* **2001**, *17*, 7620−7627.
(4) Manica, R.; Connor, J. N.; Clasohm, L. Y.; Carnie, S. L.; Horn, R. G.; Chan, D. Y. C. Transient Responses of a Wetting Film to Mechanical and Electrical Perturbations. *Langmuir* **2008**, *24*, 1381−1390.
(5) Valtiner, M.; Kristiansen, K.; Greene, G. W.; Israelachvili, J. N. Effect of Surface Roughness and Electrostatic Surface Potentials on Forces between Dissimilar Surfaces in Aqueous Solution. *Adv. Mater.* **2011**, *23*, 2294−2299.
(6) Kristiansen, K.; Valtiner, M.; Greene, G. W.; Boles, J. R.; Israelachvili, J. N. Pressure Solution - the Importance of the Electrochemical Surface Potentials. *Geochim. Cosmochim. Acta* **2011**, *75*, 6882−6892.
(7) Israelachvili, J. Thin-Film Studies Using Multiple-Beam Interferometry. *J. Colloid Interface Sci.* **1973**, *44*, 259−272.
(8) Israelachvili, J.; et al. Recent Advances in the Surface Forces Apparatus (Sfa) Technique. *Rep. Prog. Phys.* **2010**, *73*, 036601.
(9) Heuberger, M.; Luengo, G.; Israelachvili, J. Topographic Information from Multiple Beam Interferometry in the Surface Forces Apparatus. *Langmuir* **1997**, *13*, 3839−3848.
(10) Hogg, R.; Healy, T. W.; Fuerstenau, D. W. Mutual Coagulation of Colloidal Dispersions. *Trans. Faraday Soc.* **1966**, *62*, 1638−1651.
(11) Valtiner, M.; Banquy, X.; Kristiansen, K.; Greene, G. W.; Israelachvili, J. N. The Electrochemical Surface Forces Apparatus: The Effect of Surface Roughness, Electrostatic Surface Potentials, and Anodic Oxide Growth on Interaction Forces, and Friction between Dissimilar Surfaces in Aqueous Solutions. *Langmuir* **2012**, *28*, 13080−13093.
(12) Parsegian, V. A.; Gingell, D. Electrostatic Interaction across a Salt Solution between Two Bodies Bearing Unequal Charges. *Biophys. J.* **1972**, *12*, 1192−1204.
(13) Frechette, J.; Vanderlick, T. K. Electrocapillary at Contact: Potential-Dependent Adhesion between a Gold Electrode and a Mica Surface. *Langmuir* **2005**, *21*, 985−991.
(14) Barten, D.; Kleijn, J. M.; Duval, J.; von Leeuwen, H. P.; Lyklema, J.; Stuart, M. A. C. Double Layer of a Gold Electrode Probed by Afm Force Measurements. *Langmuir* **2003**, *19*, 1133−1139.
(15) Wang, J.; Bard, A. J. Direct Atomic Force Microscopic Determination of Surface Charge at the Gold/Electrolyte Interface - the Inadequacy of Classical Gcs Theory in Describing the Double-Layer Charge Distribution. *J. Phys. Chem. B* **2001**, *105*, 5217−5222.
(16) Pashley, R. M. Hydration Forces between Mica Surfaces in Electrolyte-Solutions. *Adv. Colloid Interface Sci.* **1982**, *16*, 57−62.
(17) Steigerwald, J. M.; Murarka, S. P.; Gutmann, R. J. *Chemical Mechanical Planarization of Microelectronic Materials*; Wiley: New York, 1997.
(18) Vernaz, E. Y.; Dussossoy, J. L. Current State of Knowledge of Nuclear Waste Glass Corrosion Mechanisms - the Case of R7t7 Glass. *Appl. Geochem.* **1992**, 13−22.
(19) Napoli, M.; Eijkel, J. C. T.; Pennathur, S. Nanofluidic Technology for Biomolecule Applications: A Critical Review. *Lab Chip* **2010**, *10*, 957−985.
(20) Greene, G. W.; Kristiansen, K.; Meyer, E. E.; Boles, J. R.; Israelachvili, J. N. Role of Electrochemical Reactions in Pressure Solution. *Geochim. Cosmochim. Acta* **2009**, *73*, 2862−2874.
(21) Heald, M. T. Stylolites in Sandstones. *J. Geol.* **1955**, *63*, 101−114.
(22) Alcantar, N.; Israelachvili, J.; Boles, J. Forces and Ionic Transport between Mica Surfaces: Implications for Pressure Solution. *Geochim. Cosmochim. Acta* **2003**, *67*, 1289−1304.
(23) Becker, A. Quartz Pressure Solution - Influence of Crystallographic Orientation. *J. Struct. Geol.* **1995**, *17*, 1395−1397.
(24) Weyl, P. K. Pressure Solution and the Force of Crystallization - a Phenomenological Theory. *J. Geophys. Res.* **1959**, *64*, 2001−2025.
(25) Walderhaug, O.; Bjorkum, P. A.; Aase, N. E. Kaolin-Coating of Stylolites, Effect on Quartz Cementation and General Implications for Dissolution at Mineral Interfaces. *J. Sediment. Res.* **2006**, *76*, 234−243.
(26) Rimstidt, J. D.; Barnes, H. L. The Kinetics of Silica-Water Reactions. *Geochim. Cosmochim. Acta* **1980**, *44*, 1683−1699.
(27) House, W. A.; Orr, D. R. Investigation of the Ph-Dependence of the Kinetics of Quartz Dissolution at 25-Degrees-C. *J. Chem. Soc., Faraday Trans.* **1992**, *88*, 233−241.
(28) Schmickler, W. *Interfacial Electrochemistry*; Oxford University Press: New York, 1996.
(29) Dove, P. M. The Dissolution Kinetics of Quartz in Aqueous Mixed Cation Solutions. *Geochim. Cosmochim. Acta* **1999**, *63*, 3715−3727.
(30) Landman, U.; Luedtke, W. D.; Ribarsky, M. W. Structural and Dynamical Consequences of Interactions in Interfacial Systems. *J. Vac. Sci. Technol., A* **1989**, *7*, 2829−2839.
(31) Xie, H. W.; Song, K. Y.; Mann, D. J.; Hase, W. L. Temperature Gradients and Frictional Energy Dissipation in the Sliding of Hydroxylated Alpha-Alumina Surfaces. *Phys. Chem. Chem. Phys.* **2002**, *4*, 5377−5385.

(32) Fischer, T. E. Tribochemistry. *Annu. Rev. Mater. Sci.* **1988**, *18*, 303−323.
(33) Hsu, S. M.; Zhang, J.; Yin, Z. F. The Nature and Origin of Tribochemistry. *Tribol. Lett.* **2002**, *13*, 131−139.
(34) Affatigato, M.; Osborne, D. H.; Haglund, R. F. Effect of Surface Roughness on the Acid Etching of Amorphous Silica. *J. Am. Ceram. Soc.* **1996**, *79*, 688−694.
(35) Lee, S. M.; Lee, Y. H.; Hwang, Y. G.; Hahn, J. R.; Kang, H. Defect-Induced Oxidation of Graphite. *Phys. Rev. Lett.* **1999**, *82*, 217−220.
(36) Vattuone, L.; Burghaus, U.; Savio, L.; Rocca, M.; Costantini, G.; de Mongeot, F. B.; Boragno, C.; Rusponi, S.; Valbusa, U. Oxygen Interaction with Disordered and Nanostructured Ag(001) Surfaces. *J. Chem. Phys.* **2001**, *115*, 3346−3355.
(37) Akbulut, M.; Alig, A. R. G.; Israelachvili, J. Friction and Tribochemical Reactions Occurring at Shearing Interfaces of Nanothin Silver Films on Various Substrates. *J. Chem. Phys.* **2006**, *124*, 174703.
(38) Armand, M.; Endres, F.; MacFarlane, D. R.; Ohno, H.; Scrosati, B. Ionic-Liquid Materials for the Electrochemical Challenges of the Future. *Nat. Mater.* **2009**, *8*, 621−629.
(39) Hayes, R.; Borisenko, N.; Tam, M. K.; Howlett, P. C.; Endres, F.; Atkin, R. Double Layer Structure of Ionic Liquids at the Au(111) Electrode Interface: An Atomic Force Microscopy Investigation. *J. Phys. Chem. C* **2011**, *115*, 6855−6863.
(40) Gebbie, M. A.; Valtiner, M.; Banquy, X.; Fox, E. T.; Henderson, W. A.; Israelachvili, J. N. Ionic Liquids Behave as Dilute Electrolyte Solutions. *Proc. Natl. Acad. Sci. U.S.A.* **2013**, *110*, 9674−9679.
(41) Horn, R. G.; Evans, D. F.; Ninham, B. W. Double-Layer and Solvation Forces Measured in a Molten-Salt and Its Mixtures with Water. *J. Phys. Chem.* **1988**, *92*, 3531−3537.
(42) Cummings, P. T.; Docherty, H.; Iacovella, C. R.; Singh, J. K. Phase Transitions in Nanoconfined Fluids: The Evidence from Simulation and Theory. *AIChE J.* **2010**, *56*, 842−848.
(43) Israelachvili, J. N.; Pashley, R. M. Molecular Layering of Water at Surfaces and Origin of Repulsive Hydration Forces. *Nature* **1983**, *306*, 249−250.
(44) Horn, R. G.; Israelachvili, J. N. Direct Measurement of Structural Forces between 2 Surfaces in a Non-Polar Liquid. *J. Chem. Phys.* **1981**, *75*, 1400−1411.
(45) Perkin, S.; Albrecht, T.; Klein, J. Layering and Shear Properties of an Ionic Liquid, 1-Ethyl-3-Methylimidazolium Ethylsulfate, Confined to Nano-Films between Mica Surfaces. *Phys. Chem. Chem. Phys.* **2010**, *12*, 1243−1247.
(46) Perkin, S.; Crowhurst, L.; Niedermeyer, H.; Welton, T.; Smith, A. M.; Gosvami, N. N. Self-Assembly in the Electrical Double Layer of Ionic Liquids. *Chem. Commun.* **2011**, *47*, 6572−6574.
(47) Hayes, R.; Warr, G. G.; Atkin, R. At the Interface: Solvation and Designing Ionic Liquids. *Phys. Chem. Chem. Phys.* **2010**, *12*, 1709−1723.
(48) Mezger, M.; et al. Molecular Layering of Fluorinated Ionic Liquids at a Charged Sapphire (0001) Surface. *Science* **2008**, *322*, 424−428.
(49) Galinski, M.; Lewandowski, A.; Stepniak, I. Ionic Liquids as Electrolytes. *Electrochim. Acta* **2006**, *51*, 5567−5580.
(50) Tokuda, H.; Tsuzuki, S.; Susan, M.; Hayamizu, K.; Watanabe, M. How Ionic Are Room-Temperature Ionic Liquids? An Indicator of the Physicochemical Properties. *J. Phys. Chem. B* **2006**, *110*, 19593−19600.
(51) Frink, L. J. D.; van Swol, F. Solvation Forces between Rough Surfaces. *J. Chem. Phys.* **1998**, *108*, 5588−5598.
(52) Lauw, Y.; Horne, M. D.; Rodopoulos, T.; Lockett, V.; Akgun, B.; Hamilton, W. A.; Nelson, A. R. J. Structure of [C(4)Mpyr][Ntf2] Room-Temperature Ionic Liquid at Charged Gold Interfaces. *Langmuir* **2012**, *28*, 7374−7381.
(53) de Gennes, P. G. *The Physics of Liquid Crystals*; Oxford University Press: Oxford, U.K., 1998.
(54) Gruler, H.; Meier, G. Electric Field-Induced Deformations in Oriented Liquid-Crystals of Nematic Type. *Mol. Cryst. Liq. Cryst.* **1972**, *16*, 299−310.
(55) Helfrich, W. Conduction-Induced Alignment of Nematic Liquid Crystals - Basic Model and Stability Considerations. *J. Chem. Phys.* **1969**, *51*, 4092-&.
(56) Ruths, M.; Steinberg, S.; Israelachvili, J. N. Effects of Confinement and Shear on the Properties of Thin Films of Thermotropic Liquid Crystal. *Langmuir* **1996**, *12*, 6637−6650.
(57) Zhang, X. J.; Zhang, X. H.; Xiong, Y.; Tian, Y.; Wen, S. Z. Anti-Electroviscous Effect of near-Surface 5cb Liquid Crystal and Its Boundary Lubrication Property. *Rheol. Acta 51*, 267-277.
(58) Conway, B. E. Electrochemical Oxide Film Formation at Noble-Metals as a Surface-Chemical Process. *Prog. Surf. Sci.* **1995**, *49*, 331−452.
(59) Hamelin, A.; Martins, A. M. Cyclic Voltammetry at Gold Single-Crystal Surfaces 0.2. Behaviour of High-Index Faces. *J. Electroanal. Chem.* **1996**, *407*, 13−21.
(60) Barnartt, S. The Oxygen-Evolution Reaction at Gold Anodes 0.1. Accuracy of Overpotential Measurements. *J. Electrochem. Soc.* **1959**, *106*, 722−729.
(61) Pourbaix, M. *Atlas of Electrochemical Equilibria in Aqueous Solutions*; National Association of Corrosion Engineers: Houston, TX, 1974.
(62) Donaldson, S. H.; Valtiner, M.; Gebbie, M. A.; Haradad, J.; Israelachvili, J. N. Interactions and Visualization of Bio-Mimetic Membrane Detachment at Smooth and Nano-Rough Gold Electrode Surfaces. *Soft Matter* **2013**, *9*, 5231−5238.
(63) Lee, B. P.; Messersmith, P. B.; Israelachvili, J. N.; Waite, J. H. Mussel-Inspired Adhesives and Coatings. In *Annual Review of Materials Research*; Clarke, D. R., Fratzl, P., Eds.; Annual Reviews: Palo Alto, CA, 2011; Vol. *41*, pp 99−132.
(64) Anderson, T. H.; Yu, J.; Estrada, A.; Hammer, M. U.; Waite, J. H.; Israelachvili, J. N. The Contribution of Dopa to Substrate-Peptide Adhesion and Internal Cohesion of Mussel-Inspired Synthetic Peptide Films. *Adv. Funct. Mater.* **2010**, *20*, 4196−4205.
(65) Lee, H.; Scherer, N. F.; Messersmith, P. B. Single-Molecule Mechanics of Mussel Adhesion. *Proc. Natl. Acad. Sci. U.S.A.* **2006**, *103*, 12999−13003.
(66) Kastrup, C. J., et al. Painting Blood Vessels and Atherosclerotic Plaques with an Adhesive Drug Depot. *Proc. Natl. Acad. Sci. U.S.A. 109*, 21444-21449.
(67) Haller, C. M.; Buerzle, W.; Brubaker, C. E.; Messersmith, P. B.; Mazza, E.; Ochsenbein-Koelble, N.; Zimmermann, R.; Ehrbar, M. Mussel-Mimetic Tissue Adhesive for Fetal Membrane Repair: A Standardized Ex Vivo Evaluation Using Elastomeric Membranes. *Prenatal Diagn.* **2011**, *31*, 654−660.
(68) Winslow, B. D.; Shao, H.; Stewart, R. J.; Tresco, P. A. Biocompatibility of Adhesive Complex Coacervates Modeled after the Sandcastle Glue of Phragmatopoma Californica for Craniofacial Reconstruction. *Biomaterials* **2010**, *31*, 9373−9381.
(69) Yu, J.; Wei, W.; Danner, E.; Ashley, R. K.; Israelachvili, J. N.; Waite, J. H. Mussel Protein Adhesion Depends on Interprotein Thiol-Mediated Redox Modulation. *Nat. Chem. Biol.* **2011**, *7*, 588−590.
(70) Yu, J.; Wei, W.; Menyo, M. S.; Masic, A.; Waite, J. H.; Israelachvili, J. N. Adhesion of Mussel Foot Protein-3 to Tio2 Surfaces: The Effect of Ph. *Biomacromolecules* **2013**, *14*, 1072−1077.
(71) Murgida, D. H.; Hildebrandt, P. Disentangling Interfacial Redox Processes of Proteins by Serr Spectroscopy. *Chem. Soc. Rev.* **2008**, *37*, 937−945.
(72) Mannoor, M. S.; Jiang, Z. W.; James, T.; Kong, Y. L.; Malatesta, K. A.; Soboyejo, W. O.; Verma, N.; Gracias, D. H.; McAlpine, M. C. 3d Printed Bionic Ears. *Nano Lett.* **2013**, *13*, 2634−2639.
(73) Willner, I.; Katz, E. Integration of Layered Redox Proteins and Conductive Supports for Bioelectronic Applications. *Angew. Chem., Int. Ed.* **2000**, *39*, 1180−1218.
(74) Min, Y.; Kristiansen, K.; Boggs, J. M.; Husted, C.; Zasadzinski, J. A.; Israeiachvill, J. Interaction Forces and Adhesion of Supported Myelin Lipid Bilayers Modulated by Myelin Basic Protein. *Proc. Natl. Acad. Sci. U.S.A.* **2009**, *106*, 3154−3159.
(75) Banquy, X.; Kristiansen, K.; Lee, D. W.; Israelachvili, J. N. Adhesion and Hemifusion of Cytoplasmic Myelin Lipid Membranes

Are Highly Dependent on the Lipid Composition. *Biochim. Biophys. Acta, Biomembr.* **2012**, *1818*, 402−410.
(76) Lee, D. W.; Min, Y. J.; Dhar, P.; Ramachandran, A.; Israelachvili, J. N.; Zasadzinski, J. A. Relating Domain Size Distribution to Line Tension and Molecular Dipole Density in Model Cytoplasmic Myelin Lipid Monolayers. *Proc. Natl. Acad. Sci. U.S.A.* **2011**, *108*, 9425−9430.
(77) Jahn, R.; Scheller, R. H. Snares - Engines for Membrane Fusion. *Nat. Rev. Mol. Cell Biol.* **2006**, *7*, 631−643.
(78) Chapman, E. R. How Does Synaptotagmin Trigger Neurotransmitter Release? *Annu. Rev. Biochem.* **2008**, *77*, 615−641.
(79) Jahn, R.; Fasshauer, D. Molecular Machines Governing Exocytosis of Synaptic Vesicles. *Nature* **2012**, *490*, 201−207.